UNIVERSITY OF CALIFORNIA
RIVERSIDE

Thermal Properties of Graphene and Applications for Thermal Management of High-Power Density Electronics

A Dissertation submitted in partial satisfaction
of the requirements for the degree of

Doctor of Philosophy

in

Electrical Engineering

by

Zhong Yan

December 2013

Dissertation Committee:
Dr. Alexander A. Balandin, Chairperson
Dr. Elaine Haberer
Dr. Alexander G. Khitun

The Dissertation of Zhong Yan is approved by:

_____

_____

_____

Committee Chairperson

University of California, Riverside

ACKNOWLEDGEMENTS

First and foremost, I would like to express my deep gratitude to my doctoral advisor, Professor Alexander A. Balandin for his continuous guidance, support and encouragement during the past five years. Dr. Balandin is a very wise, knowledgeable and insightful professor. His high standards on research projects and dedication to the development of both fundamental science and cutting-edge technologies are very impressive. He provided me great opportunities to work on challenging research projects and guided me to the right direct many times during my research. He also provided me many opportunities to attend conference and helped me a lot to improve my presentation skills. It really has been a great pleasure and memorable experience working under his edification .

I would like to thank all my colleagues at the Nano-Device Laboratory for their help during my research and study and for always providing a positive atmosphere in the lab. I am grateful to previous group members Dr. Guanxiong Liu, Dr Jie Yu, Dr. Craig Nolen, Dr. Desalegne Teweldebrhan, Dr.Irene Calizo, Dr. Muhammad Rahman, Dr. Suchismita Ghosh, Dr. Samia Subrina, Dr. Viveck Goyal, Dr. Zahid Hossain, and Dr. Javed Khan, as well as current members Pradumna Goli, Richard Gulotty, Chenglong Jiang, Rameez Samnakay, Jacqueline Renteria and Sylvester Ramirez for their helpful discussions and contributions towards my research work.

I am thankful to the clean room stuff Don Yan, Dexter Humphrey and Mark Heiden for the training of clean room fabrication skills and maintenance of those equipments that I used frequently during my dissertation study.

I also want to thank our research collaborators. Dr. Sergey Rumyantsev and Prof. Michal Shur at Rensselaer Polytechnic Institute (RPI) provided us some of the AlGaN/GaN devices for the graphene-graphite heat spreaders study. Prof. Alexandr Talyzin at Umeå University, Sweden provided us the GNRs-inside-SWCNTs samples for Raman spectroscopy and thermal studies.

Last but not least, I would like to express my deep gratitude to my parents, Ziliang Yan and Minggui Jiang and my wife, Xiaojie Qiang for providing their love, support, and understanding through all my educational endeavors. My father was a mechanical engineer and he encouraged me to continue my study and pursue PhD degree abroad which was an important decision in my life. My mother and my wife sacrificed a lot during these years. Without them I would not be able to achieve this. I dedicate this dissertation to them for their unconditional love and endless support.

Dedicated

to my parents

ABSTRACT OF THE DISSERTATION

Thermal Properties of Graphene and Applications for Thermal Management of High-Power Density Electronics

by

Zhong Yan

Doctor of Philosophy, Graduate Program in Electrical Engineering
University of California, Riverside, December 2013
Professor Alexander A. Balandin, Chairperson

This dissertation presents results of the experimental studies of graphene thermal properties and discusses possibilities of graphene applications for thermal management of high-power density electronic devices. The results reported here are divided into two parts. In part one, I describe fabrication and testing of graphene and few-layer graphene (FLG) heat spreaders for high-power AlGaN/GaN transistors. The mechanically exfoliated graphene-graphite layers have been transferred on top of AlGaN/GaN field-effect transistors and attached close to the heat generating regions near the metal contacts. The micro-Raman spectroscopy was used for *in situ* monitoring of the temperature of the hotspots. It was demonstrated that the temperature of the hot spots can be lowered by ~20 ℃ in transistors operating at ~13 W/mm power. The latter corresponds to an order-of-magnitude increase in the device lifetime. Simulations results supported our conclusions and indicated that graphene-graphite heat spreaders perform even better in AlGaN/GaN transistors on sapphire substrates. The proposed approach for heat removal

at micrometer and nanometer scale represents a transformative change in thermal management of electronics.

In part two of this dissertation, I report the results of investigation of thermal conductivity of thin films made of a novel nanostructured graphene material, which consists of graphene nanoribbons encapsulated in single walled carbon nanotubes. The temperature dependent Raman spectrum of this material was measured in order to obtain the temperature coefficients of G^+ peak and 2D peaks. Using the Raman optothermal technique, I determine the local temperature rise due to laser heating from the shifts in Raman peak positions. A finite element analysis method was conducted to simulated heat dissipation in the samples and to determine their effective thermal conductivity. The obtained results suggest that this hybrid graphene – carbon nanotube material can be used as fillers in thermal interface materials.

Contents

List of Figures

List of Tables

Chapter 1 Introduction and Motivations

When semiconductor industry moves into nanometer scale devices design, thermal management becomes very challenging and that might lead to the end of Moore's law. For silicon complementary metal-oxide semiconductor (Si-CMOS) technique, as the feature size shrinks, higher integration density and faster operation speed could be achieved. However, as a consequence of down scaling, modern CMOS devices consume more power and generate more heat per area and the huge local temperature rise due to Joule heating might cause devices performance degradation or even permanent damage. Besides this challenge resulting from the down scaling trend of Si based CMOS technique, thermal management is also the bottle-neck for the development of GaN based high-frequency high-power electronic devices. Owing to the high breakdown voltage and high carrier saturation velocity, GaN based transistors are outstanding candidates for radio frequency (RF) power devices and have been widely used in wireless communication. For a power device operating at particular frequency range, device feature size is fixed. However, in order to achieve as much output power as possible, dissipation power applied to this kind of device is extremely huge, resulting in huge challenge in thermal management.

1.1 Introduction: The End of Moore's Law?

In 1965, Intel co-founder Gordon Moore first observed that the number of transistors on integrated circuits (IC) had doubled every year and he predicted that this trend would

continue for the future [1]. Later on, Moore slightly altered his formulation and refined this period to roughly two years. This is the famous Moore's Law which has guided the development of semiconductor industry for over 40 years. Figure 1.1 shows the number of transistors on microprocessor as a function of the year. The vertical axis is in logarithmic scale so the curve corresponds to exponential growth over time as predicted by Moore's Law.

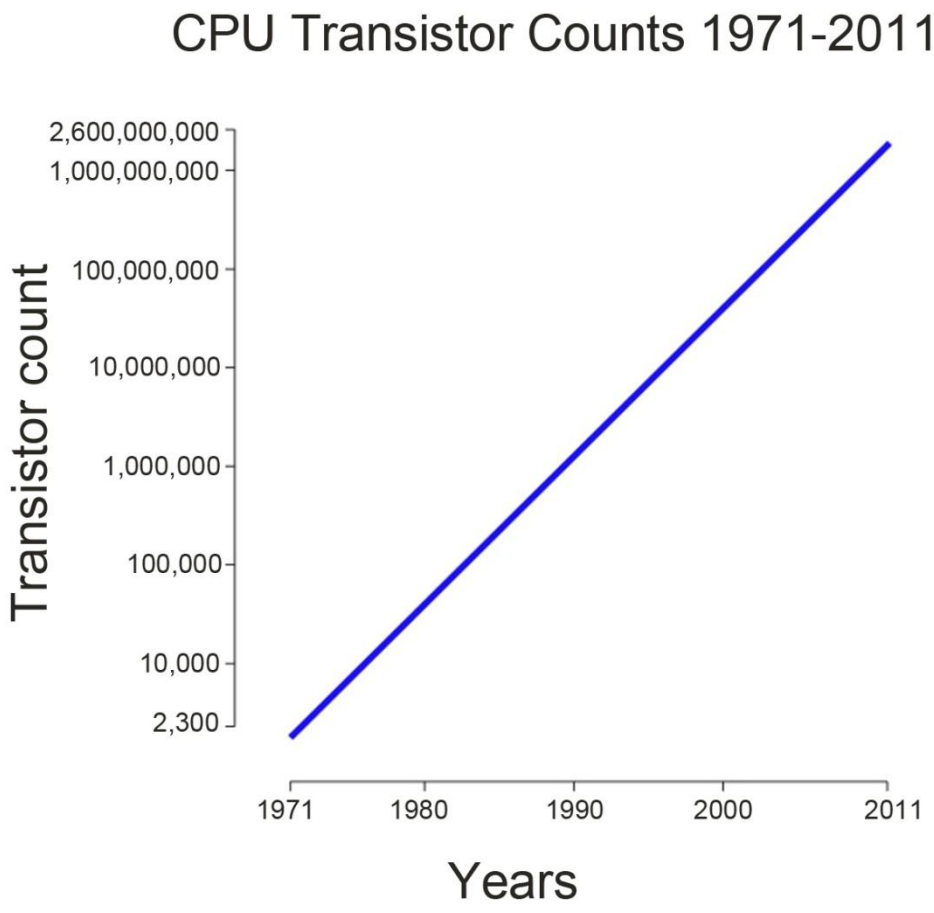

Figure 1.1 Moore's Law. CPU transistor counts as a function of the year. The figure was plotted with data extracted from http://commons.wikimedia.org/wiki/User:Wgsimon

However, Moore's Law has faced great challenge right now. Moore's Law indicates a trend of the feature size shrinking of integrated circuits and accompanying this down scaling process, the performance of IC will be improved and the cost will be reduced. Nowadays, the most advanced commercially available CPU is fabricated with 22 nanometer technology and products with 15 nanometer technology will be available very soon. 15 nm refers to the size of the smallest feature that the fabrication equipment can etch onto the surface of a wafer. Integrated circuits with higher integration density and faster working speed will consume more power and generate more heat.

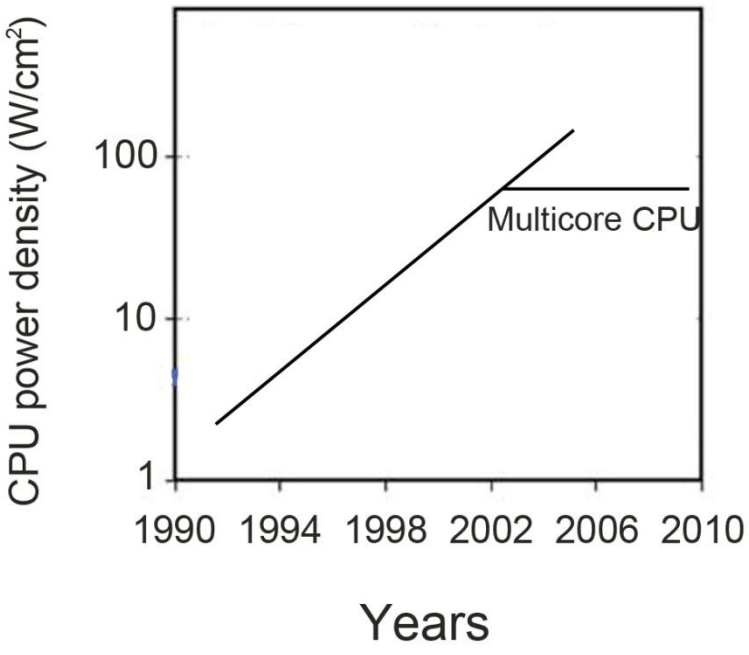

Figure 1.2 CPU power density as a function of the year. The figure was plotted according to data extracted from reference [2]

Figure 1.2 shows the CPU power density as a function of the year. An exponential trend of increasing power density is an inevitable consequence of Moore's Law. The

current level of on-chip power density has reached the order of 100 W/cm^2, which is on the same order of magnitude of a nuclear reactor. The semiconductor industry will soon reach the limit of heat dissipation which might lead to the end of Moore's Law [3].

1.2 Motivations: Graphene Heat Spreaders

Addressing those problems arising from the increasing heat dissipation in modern electronic devices requires systematic multidisciplinary work which will involve scientists and engineers both in academia and semiconductor industry. For example, physicists need to provide a better picture of thermal transport in nanometer scale devices; material science engineers are trying to find new materials to either replace or improve the performance of conventional heat sink and thermal interface materials (TIM); engineers at semiconductor industry keep trying to optimize their package design to facilitate heat removal.

Among all those efforts, finding new materials with high thermal conductivity as heat spreaders is an attractive approach to improve heat removal capability of modern electronic devices. There are several basic requirements of this new material. First of all, it must have extremely high thermal conductivity. Second, since silicon based CMOS technique will not be replaced in the near future, this new material must be compatible for integration with current Si-CMOS technology. Last, the cost must be acceptable in order to develop a commercial product. A new material called graphene is a promising candidate for the heat removal applications.

Graphene is one atomic-layer thin film of carbon atoms packed in honeycomb lattice.

It has attracted intensive interest both in academia and industry ever since its experimental discovery in 2004 [4]. Graphene is the thinnest material known so far with the strongest mechanical property ever measured [5]. It has extraordinary electronic band structure and extremely high carrier mobility [4, 6].

Moreover, graphene also has outstanding thermal properties. The intrinsic thermal conductivity of suspended single layer graphene (SLG) has been measured around 3000~5000 W/mK [7]. For few layer graphene (FLG), the thermal conductivity value decreases with number of layers [8] and will soon approach bulk graphite limit, which is around 2000 W/mK. This is still a very high value. Table 1.1 compares thermal conductivities of graphene with other carbon materials and materials commonly used in semiconductor devices. High thermal conductivity leads to good heat removal capability. In addition, graphene films can maintain high thermal conductivity when the thickness reduce to nanometer scale while thermal conductivity of metal films rapidly decrease with film thickness [9, 10]. For many technologically important metals, for example, aluminum, copper or gold, the thermal conductivity of the metal film constitutes only ~20% of the bulk value at the film thickness ~100 nm.

The planar two-dimensional geometry of graphene enables conventional lithography and etching techniques used in semiconductor industry, which gives graphene a great advantage in terms of compatibility compared with other high-thermal-conductivity material like carbon nanotubes. And the recent progress in the chemical vapor deposition (CVD) growth of graphene led to fabrication of large-area graphene layers that are transferable onto various insulating substrates [11, 12]. The CVD grown graphene layers

of up to 30 inches in size on cheap flexible substrates have been demonstrated [11]. Various methods of graphene synthesis were reported [13, 14]. We can expect that a reliable method to synthesize high-quality large-scale graphene film will be developed in the near future and the mass production of graphene will be available in semiconductor industry. All above reasons explain why we are interested in graphene heat spreaders.

Table 1.1: Room temperature thermal conductivity values of common materials used in semiconductors and thermal conductivity values of carbon materials

Materials	Room Temp Thermal Conductivity
Single Layer Graphene	~3000~5300 W/mK [7]
Bi-layer to Few Layer Graphene	~2800 W/mk to ~1300 W/mk
Silicon (Si)	145 W/mK
SiO_2	1 - 13 W/mK
Copper	400 W/mK
Gold	~300 W/mk
Diamond	1000 - 2200 W/mK
Graphite	200 - 2000 W/mK (Orientation Dependent)
Diamond-like Carbon (DLC)	0.1 - 10 W/mK
Carbon Nano-tubes (CNTs)	3000 - 3500 W/mK

1.3 Overview

The outline of my dissertation is as follows: Chapter 2 briefly reviews the discovery of graphene and gives brief introductions to the extraordinary properties of graphene. Chapter 3 systematically presents the experimental results of proof-of-concept demonstration of utilizing graphene-graphite heat spreaders for thermal management of high-power AlGaN/GaN HFETs. Chapter 4 presents the Raman spectroscopy and thermal properties of a novel nanostructured material- graphene nanoribbons encapsulated in single-walled carbon nanotubes. Chapter 5 is the summary of my dissertation.

REFERENCES

[1] G. E. Moore, Electronics **38** (1965).

[2] E. Pop, Nano Research **3**, 147 (2010).

[3] L. B. Kish, Physics Letter A **305** (2002).

[4] K. S. Novoselov, A. K. Geim, S. V. Morozov, D. Jiang, Y. Zhang, S. V. Dubonos, I. V. Grigorieva, and A. A. Firsov, Science **306**, 666 (2004).

[5] C. Lee, X. Wei, J. W. Kysar, and J. Hone, Science **321**, 385 (2008).

[6] K. S. Novoselov, A. K. Geim, S. V. Morozov, D. Jiang, M. I. Katsnelson, I. V. Grigorieva, S. V. Dubonos, and A. A. Firsov, Nature **438**, 197 (2005).

[7] A. A. Balandin, S. Ghosh, W. Bao, I. Calizo, D. Teweldebrhan, F. Miao, and C. N. Lau, Nano Letters **- 8** (2008).

[8] S. Ghosh, W. Bao, D. L. Nika, S. Subrina, E. P. Pokatilov, C. N. Lau, and A. A. Balandin, Nat Mater **9**, 555 (2010).

[9] P. Nath and K. L. Chopra, Thin Solid Films **20**, 53 (1974).

[10] G. Chen and P. Hui, Applied Physics Letters **74**, 2942 (1999).

[11] S. Bae, H. Kim, Y. Lee, X. Xu, J.-S. Park, Y. Zheng, J. Balakrishnan, T. Lei, H. Ri Kim, Y. I. Song, Y.-J. Kim, K. S. Kim, B. Ozyilmaz, J.-H. Ahn, B. H. Hong, and S. Iijima, Nat Nano **5**, 574 (2010).

[12] X. Li, W. Cai, J. An, S. Kim, J. Nah, D. Yang, R. Piner, A. Velamakanni, I. Jung, E. Tutuc, S. K. Banerjee, L. Colombo, and R. S. Ruoff, Science **324**, 1312 (2009).

[13] W. A. de Heer, C. Berger, X. Wu, P. N. First, E. H. Conrad, X. Li, T. Li, M. Sprinkle, J. Hass, M. L. Sadowski, M. Potemski, and G. Martinez, Solid State Communications **143**, 92 (2007).

[14] L. Zhang, J. Liang, Y. Huang, Y. Ma, Y. Wang, and Y. Chen, Carbon **47**, 3365 (2009).

Chapter 2 Background: Properties of Graphene and Sample Preparation

The discovery of graphene is like a supernova in material science and condensed matter physics. It has attracted enormous interest in both academia and industry, triggering a scientific gold rush among physicists, chemists, material scientists and electrical engineers throughout the world. This chapter gives brief review of the discovery of graphene and those extraordinary properties of graphene.

2.1 Graphene Discovery

Theoretical investigation of electrical property of graphene was first conducted back in 1940s [1] and continued in 1950s [2, 3], almost sixty years ahead of the experimental discovery of that material. The purpose of those studies was to understand electronic properties of graphite, which became an important material for nuclear reaction. It had been predicted that pure two-dimensional crystal could not exist in the real world due to thermodynamic unstable [4, 5]. However, graphene has been experimentally discovered by Dr. Geim and Dr. Novoselov in 2004 [6] with a relatively simple method, namely mechanical exfoliation method. They used adhesive tape to repeatedly split graphite crystals into thinner pieces and then the flakes were transferred to a silicon wafer with 300 nm oxide layer on top. Single layer graphene flakes on the substrate could be identified under optical microscope through small but noticeable optical contrast. The

existence of graphene and other recently discovered one-atomic-layer crystals does not contradict with the thermodynamics theory. It can be argued that those materials supported by a substrate are not free standing 2D crystals and the extracted 2D crystals become intrinsically stable by gentle crumpling in the third dimension [7, 8]. Such 3D warping leads to a gain in elastic energy but suppresses thermal vibrations, which above a certain temperature can minimize the total free energy [8]. The Nobel Prize in Physics for 2010 was awarded to Dr. Geim and Dr. Novoselov at the University of Manchester "for groundbreaking experiments regarding the two-dimensional material graphene" .

2.2 Atomic Structure and Unique Electronic Properties of Graphene

Graphene is a monolayer of sp^2 bonded carbon atoms arranged in a hexagonal crystal structure. It can be viewed as the basic building block for sp^2 bonded carbon allotropes. It can be wrapped up into 0D fullerenes (C_{60}), rolled into 1D nanotubes and stacked into bulk graphite. Figure 2.1 shows the schematics of the atomic structure of graphene, fullerenes and carbon nanotubes. The distance between two nearest sp^2 bonded carbon atoms is 1.42 Å.

The electronic property of graphene differs from most three dimensional materials. Intrinsic graphene is a semimetal with zero band gap. It has been theoretically studied as early as 1947 [1]. Due to the hexagonal crystal structure, the reciprocal lattice of graphene is also hexagonal (shown in Figure 2.2). At the six corners of the first Brillouin

zone, the electron energy versus momentum, E-k, relation is linear [9, 10]. This linear dispersion leads to zero effective mass of electrons and holes near those six points. Electrons and holes behave like relativistic particles described by the Dirac equation for spin -1/2 particles . Hence, the electrons and holes are called Dirac fermions and the six corners of the Brillouin zone are called the Dirac points. Graphene reveals ambipolar electric field effect that the charge carrier types can be turned continuously from electrons to holes. Experimental results show that graphene has extremely high electron mobility at room temperature, up to 15,000 $cm^2 \cdot V^{-1} s^{-1}$ [10] and this value is still limited by impurity scattering. The intrinsic carrier mobility at room temperature limited by acoustic phonon scattering of graphene could achieve 200,000 $cm^2 \cdot V^{-1} s^{-1}$ at a carrier density of 10^{12} cm^{-2} [11]. Owing to its high carrier mobility, graphene has attracted intensive attention as promising candidate for new-generation high-frequency electronics. Graphene transistors with cut-off frequency above 100 GHz have been experimentally demonstrated [12, 13].

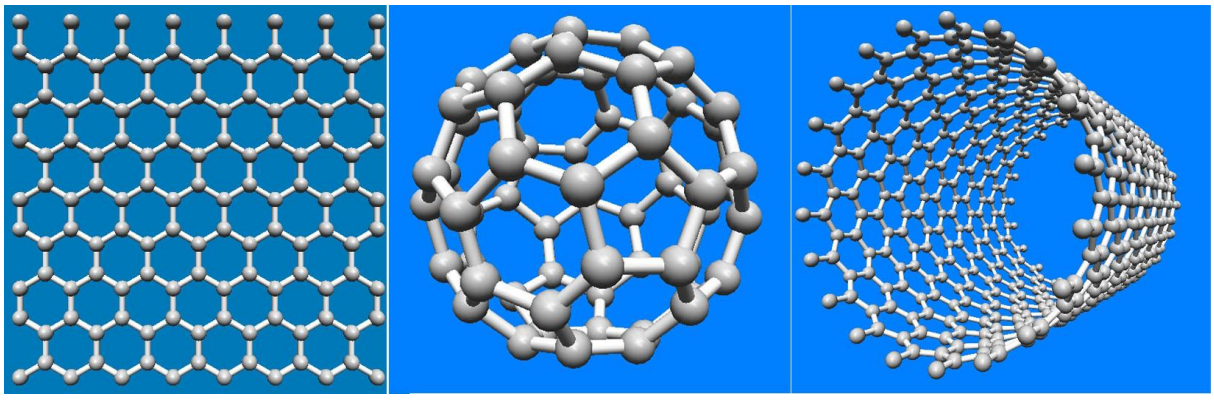

Figure 2.1 Atomic structure of graphene (left), fullerenes (C_{60}, middle) and carbon nanotubes (right)

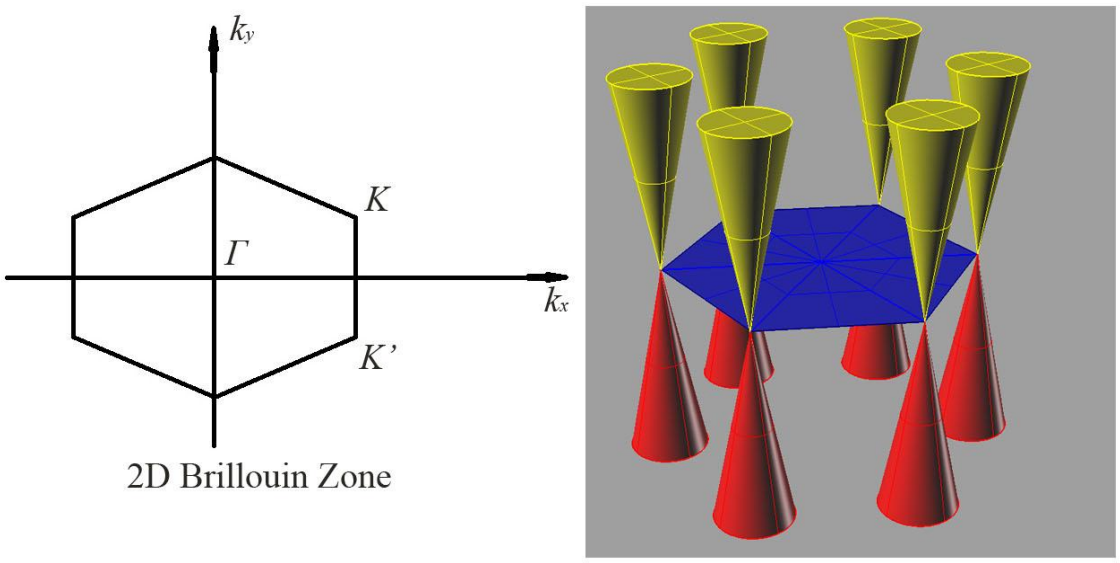

Figure 2.2 The first Brillouin zone of graphene and electronic band structure.

2.3 Graphene Production: From Mechanical Exfoliation to Chemical Growth

Graphene was first obtained experimentally in 2004 through mechanical exfoliation method. The graphene sample preparation starts from peeling thinner graphite flakes from bulk material. Bulk graphite can be viewed as monolayer graphene stacked layer by layer. The chemical bonding between sp^2 bonded carbon atoms in graphene layer are very strong. However, the bonding between two nearby graphene layers is week van der Waals force and could be easily broken by external force. By using adhesive tape repeatedly split graphite flakes into thinner pieces, optically transparent thin flakes could be obtained. Then the tape with thin graphite flakes is attached to a silicon substrate with 300 nm silicon dioxide layer on top and pressed gently for few minutes. After removing

the tape many graphene flakes with random size, shape and thickness could be found on the Si substrate. This method is also named as scotch tape method or drawing method.

Figure 2.3 shows an typical optical microscope image of graphene samples fabricated in our lab with mechanical exfoliation method. The thickness of graphene flakes could be roughly estimated by the color and optical contrast under optical microscope image. As shown in Figure 2.3, thick graphene flake is almost opaque with dark green color; thin graphene flake is almost transparent. However, in order to identify the number of atomic layers in graphene flakes, other approach like Raman spectroscopy need to be applied.

Mechanical exfoliation is a very straight-forward method and can provide high quality graphene flakes up to 100 μm in size. After many years of the graphene discovery, graphene samples fabricated with this method are still widely used in research labs. However, the drawbacks of mechanical exfoliation method are also pronounced. The process of mechanical exfoliation and following graphene identification is time consuming and requires lots of man power. The thickness of graphene cannot be controlled and large, uniform graphene flakes above 100μm in size are hard to obtain with this method. Those drawbacks prevent graphene fabricated with this method from industry applications.

Recently, chemical epitaxial growth methods have been developed rapidly for graphene preparation. One method is to heat silicon carbide (SiC) to high temperatures (>1, 100 ℃) under low pressures (~10^{-6} torr) to reduce it to graphene [14]. Dimensions of epitaxial graphene grown by this process strongly depend upon the size of the SiC

substrate. The face of the SiC used for graphene formation, silicon- or carbon-terminated, highly influences the thickness, mobility and carrier density of the graphene.

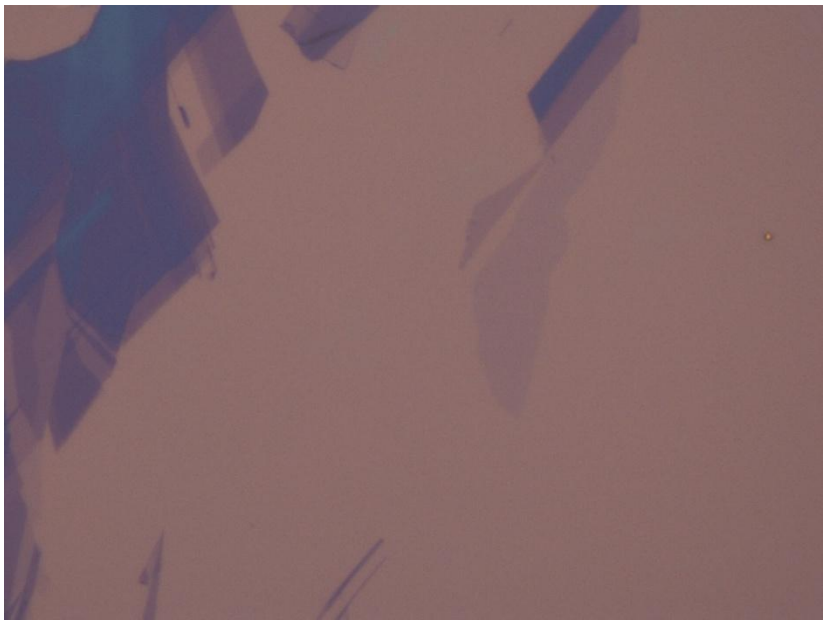

Figure 2.3 Optical microscope image of graphene sample prepared by mechanical exfoliation method in the Nano-Device Laboratory, UCR.

Another approach is epitaxial growth of graphene on metal substrates. This method use sources and the atomic structure of metal to seed graphene growth. High-quality sheets of few-layer graphene have been synthesized via chemical vapor deposition on thin nickel films with methane as a carbon source. These graphene sheets have been successfully transferred to various substrates, demonstrating viability for numerous electronic applications [15, 16]. Epitaxial growth of graphene enables potential applications of graphene in semiconductor industry. The first prototype of a graphene-based touch-screen panel from this process was demonstrated at the Computer

Electronics Show in Las Vegas, 2010 [15] as well as the development of a prototype of a flexible transparent graphene-based electrode.

2.4 Raman Spectroscopy of Graphene

Raman spectroscopy is a nondestructive, high-throughput technique widely used in material characterization. Raman scattering is an inelastic light scattering effect induced by interaction between photons and atoms or molecules. When light is scattered by a medium, most photons are elastically scattered (Rayleigh scattering), in which the scattered photons have the same energy and frequency as the incident photons. However, a small portion of scattered photons have different energy or frequency from the incident photons and the energy difference between scatter photons and incident photons corresponds to an excitation energy of the medium. In solid materials, this excitation energy corresponds to the atoms vibration modes, namely phonons.

Raman spectroscopy has been widely applied to study the electronic and structural properties of carbon based material such as graphite [17], diamond [18] and carbon nanotubes [19, 20]. Raman spectroscopy of graphene has attracted intensive research interest since the discovery of graphene [21, 22]. Figure 2.4 compares Raman spectrum of bulk graphite, single-layer graphene and bi-layer graphene (BLG). The wavelength of Raman excitation laser is 488nm. Bulk graphite has two major Raman peaks, G peak at ~ 1580 cm^{-1} and 2D band at ~ 2750 cm^{-1} and G peak intensity is much higher than 2D band. In SLG, the peak intensity ratio of 2D band over G peak is around 3~4 under 488

excitation laser. And 2D band of SLG is sharp and symmetric which can be fitted by a single Lorenzian peak. In BLG, the peak intensities of 2D band and G peak are roughly equal and the 2D band consists of four Lorenzian peaks.

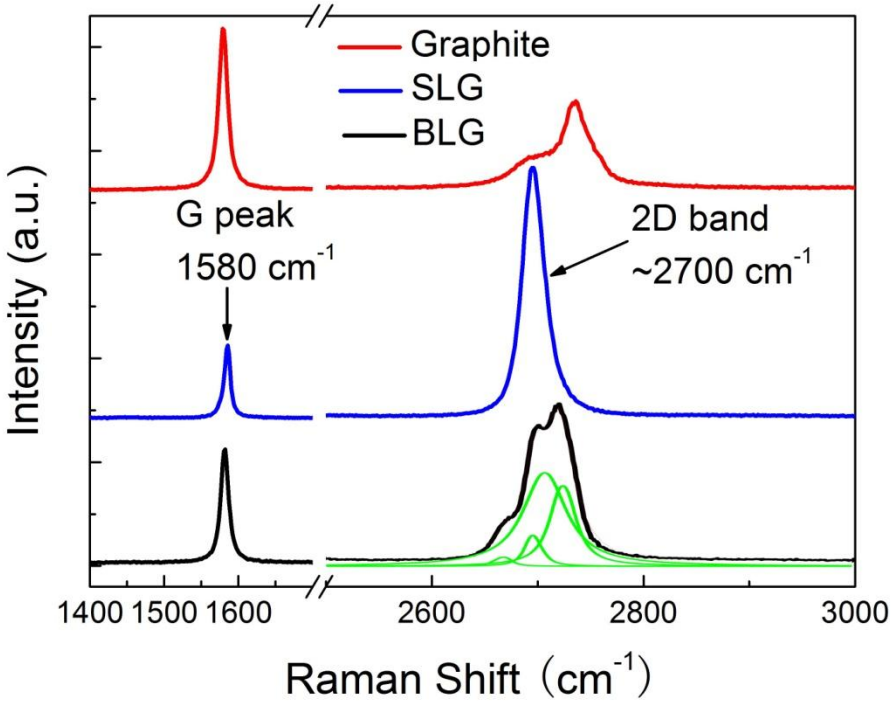

Figure 2.4 Raman spectra of bulk graphite, single layer graphene (SLG) and bi-layer graphene (BLG) measured with 488 nm Raman laser. 2D band of BLG can be fitted by four Lorenzian peaks.

For some graphene samples, a weak Raman peak at ~ 1350 cm^{-1} could be seen in the Raman spectrum. This peak is named as D peak and relates to defects in graphene crystal. Theoretically, G peak corresponds to a Brillouin zone center phonon mode while D peak corresponds to a zone boundary phonon which is prohibited by Raman selection rule. The

presence of defects break crystal symmetry and make D mode Raman active, thus the absence of D peak indicates good crystal quality for graphene samples.

2D band of graphene results from the double resonance Raman process of D mode and is strongly related to the electronic band structure of graphene. The shape of 2D band varies distinctively with number of atomic layers in few layer graphene and thus provides us a powerful tool to identify the number of graphene layers [23].

In addition, the temperature dependence of G peak frequency in the Raman spectrum of graphene has been well studied [23]. In the studied temperature range from -190 ^{o}C to 100 ^{o}C, graphene G peak shifts to lower wavenumber range (red shift) and approximately follows a liner relation. The temperature coefficient of single layer graphene has been measured as -0.015 $cm^{-1}/\ ^{o}C$. With this well established temperature coefficient, Raman spectroscopy could be applied as a thermometer to detect local temperature rise in graphene flakes by measuring the shift of Raman peak positions.

To conclude, Raman spectroscopy is a very powerful tool in graphene research. It provides non-destructive, high-throughput method to identify the number of graphene layers; it gives information about the crystal quality of graphene samples; it could also be applied as thermometer to measure temperature rise in graphene.

2.5 Superior Thermal Conductivity of Graphene

Thermal conductivity describes the capability of a material to contact heat. It is introduced through Fourier's Law, $\vec{q} = -K\nabla T$, where $\vec{q}$ is heat flux, K is thermal

conductivity and ∇T is temperature gradient. In solid material, heat is conducted by acoustic phonons as well as electrons, thus $K = K_p + K_e$, where K_p and K_e are the phonon and electron contributions respectively. In metals, thermal conductivity is dominated by K_e due to large carrier concentrations. Heat conduction in sp^2 bonded carbon allotropes is usually dominated by K_p, even for graphite which is a good electrical conductor like metal.

Although theoretical studies suggested that graphene might have unusually high thermal conductivity [24], experimental measurement of thermal conductivity of atomic layer thin film like graphene could be very challenging. Dr. Balandin and his co-workers developed an optothermal Raman technique and first measured the thermal conductivity of suspended single layer graphene [25]. The suspended graphene flake was heated up by Raman excitation laser and the temperature rise, ΔT, at different laser power, ΔP, was determined through the peak position shift of graphene Raman modes. Given the correlations between ΔT and ΔP as well as the geometry of tested graphene samples, thermal conductivity, K, could be calculated by solving heat diffusion equation. The obtained K value exceeds ~3,000 W/mK at room temperature, that is above bulk graphite limit and is among the highest values obtained experimentally [26].

Intrinsic thermal conductivity of graphene is limited by anharmonic phonon-phonon scattering, namely Umklapp scattering. The data obtained from suspended graphene is close to the intrinsic value. Thermal conductivities measured from graphene samples supported on substrate could be much lower due to coupling to the substrate and phonon scattering at the substrate defects and impurities. Measurements for exfoliated graphene

on SiO_2/Si revealed an in-plane *K* of ~600 W/mK near room temperature [27]. Thermal conductivity of graphene nanoribbons may reduce substantially due to phonon-boundary scattering. Experimental studies for graphene nanoribbons with less than five atomic planes and a width between 16 nm and 52 nm found *K* values in the range of 1,000~1,400 W/mk near room temperature [28].

The evolution of thermal properties of FLG with increasing number of layers is of great importance to understand the heat conduction in low-dimensional systems. Experimental investigation with optothermal Raman technique revealed that *K* of suspended FLG decreases with increasing number of layers, approaching the bulk graphite limit [29]. This evolution of *K* was explained by considering the intrinsic quasi-2D crystal properties described by the phonon Umklapp scattering. As number of layers in FLG increases, the phonon dispersion changes and more phase-space states become available for phonon scattering leading to a decrease in *K*. However, thermal conductivity values of FLG, varying from ~1300 W/mK to ~2800 W/mk, are still higher than most semiconductor materials and metals.

2.6 Summary

Chapter 2 briefly reviews the discovery of graphene and gives brief introductions to the extraordinary properties of graphene, including the atomic structure, electronic band structure, graphene sample preparations, Raman spectroscopy and thermal properties. The outstanding thermal properties of graphene explain the motivation of using graphene

for heat removal applications and Raman spectroscopy is the most important technique applied in this dissertation study.

REFERENCES

[[1] P. R. Wallace, Physical Review **71**, 622 (1947).

[2] J. W. McClure, Physical Review **104**, 666 (1956).

[3] J. C. Slonczewski and P. R. Weiss, Physical Review **109**, 272 (1958).

[4] L. Landau, Physikalische Zeitschrift der Sowjetunion **11**, 26 (1937).

[5] N. D. Mermin, Physical Review **176**, 250 (1968).

[6] K. S. Novoselov, A. K. Geim, S. V. Morozov, D. Jiang, Y. Zhang, S. V. Dubonos, I. V. Grigorieva, and A. A. Firsov, Science **306**, 666 (2004).

[7] J. C. Meyer, A. K. Geim, M. I. Katsnelson, K. S. Novoselov, T. J. Booth, and S. Roth, Nature **446**, 60 (2007).

[8] D. R. Nelson, T. Piran, and S. Weinberg, *Statistical Mechanics of Membranes and Surfaces* (World Scientific Singapore, 2004).

[9] J. C. Charlier, P. C. Eklund, J. Zhu, and A. C. Ferrari, in *Carbon Nanotubes* (Springer Berlin Heidelberg, 2008), Vol. 111, p. 673.

[10] A. K. Geim and K. S. Novoselov, Nat Mater **6**, 183 (2007).

[11] J.-H. Chen, C. Jang, S. Xiao, M. Ishigami, and M. S. Fuhrer, Nat Nano **3**, 206 (2008).

[12] Y. Wu, Y.-m. Lin, A. A. Bol, K. A. Jenkins, F. Xia, D. B. Farmer, Y. Zhu, and P. Avouris, Nature **472**, 74 (2011).

[13] J. Zheng, L. Wang, R. Quhe, Q. Liu, H. Li, D. Yu, W.-N. Mei, J. Shi, Z. Gao, and J. Lu, Sci. Rep. **3** (2013).

[14] P. Sutter, Nat Mater **8**, 171 (2009).

[15] S. Bae, H. Kim, Y. Lee, X. Xu, J.-S. Park, Y. Zheng, J. Balakrishnan, T. Lei, H. Ri Kim, Y. I. Song, Y.-J. Kim, K. S. Kim, B. Ozyilmaz, J.-H. Ahn, B. H. Hong, and S. Iijima, Nat Nano **5**, 574 (2010).

[16] K. S. Kim, Y. Zhao, H. Jang, S. Y. Lee, J. M. Kim, K. S. Kim, J.-H. Ahn, P. Kim, J.-Y. Choi, and B. H. Hong, Nature **457**, 706 (2009).

[17] P. Tan, Y. Deng, and Q. Zhao, Physical Review B **58**, 5435 (1998).

[18] H. Herchen and M. A. Cappelli, Physical Review B **43**, 11740 (1991).

[19] A. M. Rao, E. Richter, S. Bandow, B. Chase, P. C. Eklund, K. A. Williams, S. Fang, K. R. Subbaswamy, M. Menon, A. Thess, R. E. Smalley, G. Dresselhaus, and M. S. Dresselhaus, Science **275**, 187 (1997).

[20] M. S. Dresselhaus, G. Dresselhaus, R. Saito, and A. Jorio, Physics Reports **409**, 47 (2005).

[21] A. C. Ferrari, J. C. Meyer, V. Scardaci, C. Casiraghi, M. Lazzeri, F. Mauri, S. Piscanec, D. Jiang, K. S. Novoselov, S. Roth, and A. K. Geim, Physical Review Letters **97** (2006).

[22] Z. Ni, Y. Wang, T. Yu, and Z. Shen, Nano Research **1**, 273 (2010).

[23] I. Calizo, A. A. Balandin, W. Bao, F. Miao, and C. N. Lau, Nano Letters **7**, 2645 (2007).

[24] N. Mingo and D. A. Broido, Physical Review Letters **95**, 096105 (2005).

[25] A. A. Balandin, S. Ghosh, W. Bao, I. Calizo, D. Teweldebrhan, F. Miao, and C. N. Lau, Nano Letters **- 8** (2008).

[26] A. A. Balandin, Nat Mater **10**, 569 (2011).

[27] J. H. Seol, I. Jo, A. L. Moore, L. Lindsay, Z. H. Aitken, M. T. Pettes, X. Li, Z. Yao, R. Huang, D. Broido, N. Mingo, R. S. Ruoff, and L. Shi, Science **328**, 213 (2010).

[28] R. Murali, Y. Yang, K. Brenner, T. Beck, and J. D. Meindl, Applied Physics Letters **94**, 243114 (2009).

[29] S. Ghosh, W. Bao, D. L. Nika, S. Subrina, E. P. Pokatilov, C. N. Lau, and A. A. Balandin, Nat Mater **9**, 555 (2010).

Chapter 3: Graphene Heat Spreaders for High-Power GaN Transistors

Self-heating is a critical issue for high-power gallium nitride (GaN) electronic and optoelectronic devices. Various thermal management solutions, for example, flip-chip bonding or composite substrates, have been attempted. However, temperature rise due to dissipated power still limits the performance of GaN based high-power devices. Here we demonstrates that thermal management of GaN transistors can be substantially improved via introduction of alternative heat-escaping channels implemented with few-layer graphene—an excellent heat conductor. The graphene-graphite heat spreaders were formed on top of AlGaN/GaN transistors on SiC substrates. Using micro-Raman spectroscopy for in situ monitoring we demonstrated that temperature of the hotspots can be lowered by ~20 ℃ in transistors operating at ~13 W/mm , which corresponds to an order-of-magnitude increase in the device lifetime. Simulations results support our experimental data and indicate that graphene quilts perform even better in GaN devices on sapphire substrates. The proposed local heat spreading with materials that preserve their thermal properties at nanometre scale represents a transformative change in thermal management.

3.1 Motivations: Thermal Issues of GaN Based High-Power Transistors

Gallium nitride (GaN) based heterostructure field-effect transistors (HFETs) are attractive devices for high-frequency high-power applications [1, 2]. Commercial products of AlGaN/GaN HFETs emerged in 2005 and have developed rapidly since then. They have been widely used as power amplifiers or switches in wireless communications and radars. AlGaN/GaN HFETs possess high breakdown voltage [3], which allows high drain voltage to be used. The high sheet charge carrier concentration and large saturation velocity lead to high saturation current density. Therefore input power density of AlGaN/GaN HFETs, measured in watts per millimeter of gate width, could be extremely high, resulting in high output power. Amplifiers fabricated using AlGaN/GaN HFETs have produced RF power over a wide frequency range up to several hundred watts [4, 5]. However, these high power densities inevitably lead to huge amount of heat generation and present extreme power dissipation demands.

Thermal management is a critical issue for the designers of GaN based high-power devices. Device temperature rise due to Joule heating might lead to severe performance degradation and reliability issues. Performance degradation of GaN transistors observed at elevated device temperature includes degradation of dc drain current, gain and output power, as well as an increase in the gate leakage current [6]. Moreover, the mean time to failure (MTTF) of GaN transistors decrease exponentially with operation temperature increase [6]. For commercial products of AlGaN/GaN HFETs, a reasonable lifetime is around 10^6 hours and correspondingly, the operation temperature should be lower than

180 ^{o}C. The absolute thermal resistance of a particular device is decided by the heat removal capability and there is a simple relation between the dissipation power and device temperature rise: $\Delta T = P_{dis} \cdot R_{th}$, where R_{th} is thermal resistance in K/W and P_{dis} is dissipation power. If ΔT is fixed at 180^{o}C, the maximum dissipation power is limited by thermal resistance, thus the output power is also limited by heat removal capability. Thermal management is the bottle-neck for further increasing output power of AlGaN/GaN HFETs.

Experimental studies and simulation results all prove that non-uniform distribution of dissipated power in GaN transistors leads to the formation of micrometer scale hotspots near device channels [7, 8] and over-heating at those hotspots directly induce performance degradation or even permanent damage. A large number of methods have been used to improve heat removal from GaN devices. The sapphire substrates, with low thermal conductivity around 30 W/mk at room temperature, have been replaced by SiC substrates, which have thermal conductivity around 350 W/mk. SiC is more expensive and even in GaN transistors on SiC substrate, self-heating can lead to temperature rises, ΔT, above 180 ℃. The composite substrates [9] and flip-chip bonding [10, 11] were utilized to improve the heat removal by reducing the overall thermal resistance on the scale of the whole wafer. Despite those efforts, no approaches aim to deal with micrometer scale hotspots directly.

Here I proposed a target-cooling approach that by placing micrometer scale heat spreaders close to the hotspots, the temperature rise at hotspots would be reduced substantially. And I made proof-of-concept demonstration with AlGaN/GaN HFETs that

hotspots temperature of tested device can be substantially reduced via introduction of the top-surface heat spreaders made of few-layer graphene (FLG). Thermal conductivity of FLG, which is around 2,000 W/mK, is an order of magnitude higher than that of GaN, which ranges from ~125 to ~225 W/mk at room temperature [12, 13].The thermal conductivity of FLG is also higher than that of any metals used as heat spreaders or heat sinks in semiconductor devices. FLG films preserve their excellent heat conduction properties even when their thickness decrease to only a few nanometers. Contrary to FLG, the thermal conductivity of thin metal films, which is dominated by electrons rather phonons, reduces rapidly with decreasing film thickness. Ideally, the heat spreader should be made from material with the highest K as possible. We already know that intrinsic thermal conductivity of single layer graphene is highest. However, for heat spreaders applications, FLG is better than single layer graphene because SLG has limited cross-section area which forbids large in-plan heat flux. In addition, thermal conductivity of FLG is less subject to deterioration due to extrinsic effects, for example, defects and disorders at the interface.

The demonstrated approach for the thermal management of high-power density devices is conceptually different from conventional techniques in a sense that it specifically targets the hotspots at nanometer and micrometer scale. Instead of trying to further reduce the thermal resistance, R_{th}, of the whole substrate, we introduce the local lateral heat spreaders on top of the GaN device structure, which provide additional heat escape channels from the hotspots. Progress in graphene-FLG synthesis and transferring

graphene films onto arbitrary substrates suggests that the proposed heat spreaders can become technologically and economically feasible in the near future.

3.2 Structures and I-V Characteristics of Tested AlGaN/GaN HFET

The AlGaN/GaN HFETs tested in this study were provided to us by our collaborators from Rensselaer Polytechnic Institute (RPI). They have layered structure consisting of 30 nm $Al_{0.2}Ga_{0.8}N$ barrier layer, which was doped with silicon approximately to 2×10^{18} cm^{-3} and 0.5 μm thick GaN layer deposited on insulating 4H-SiC substrate. The device epilayer structure was grown by low-pressure metal organic chemical vapor deposition (MOCVD) method. Ohmic contacts for source and drain were fabricated using Ti (200 Å)/Al (500 Å)/Ti (200 Å)/Au (1500 Å). For the MOSFET structure, a 10 nm SiO layer was deposited on part of the heterostructure using plasma enhanced chemical vapor deposition prior to the gate fabrication. Ni (200 Å)/Au (1000 Å) were then deposited in between the source–drain electrodes to form gate electrodes. Figure 3.1 shows the schematics and optical image of the tested double gate-finger HFET device. Gate length and widths are 3.5 μm and 90 μm, respectively. Source drain separation is 12 μm. More details about AlGaN/GaN HFETs fabrication could be found in reference [14, 15].

DC current-voltage (I-V) characteristics of the AlGaN/GaN HFETs have been tested and a typical result is shown in Figure 3.2 (a). The gate bias changed from 2 V to −4 V in −2 V steps and at each step drain bias was scanned from 0V to 20V. The tested device

was completely pinched off at negative gate bias $V_G = -4$ V. The maximum source–drain current density of I_{DS} = 0.75 A/mm was obtained at a positive gate bias V_G = 2 V. The negative slope regions in I-V curves indicate a performance degradation due to Joule heating as the dissipated power increases. Those measurement were conducted at room temperature.

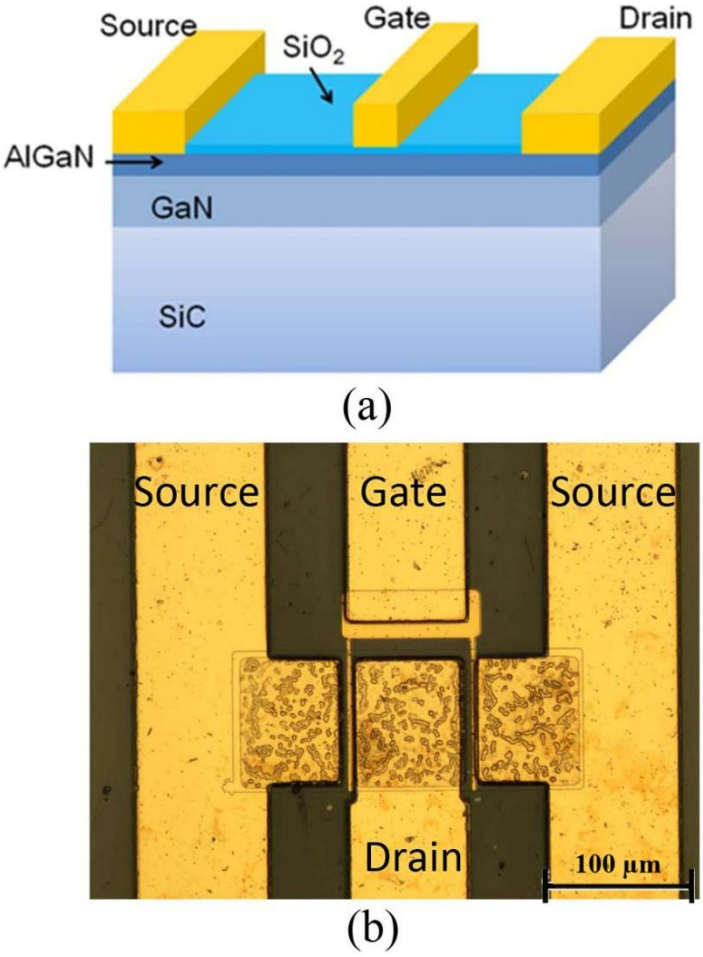

Figure 3.1 (a) Schematics of the layered structure of tested AlGaN/GaN HFET device. (b) Optical image of the tested two-finger device. Gate width is 90 µm. Scale bar is 100 µm.

The I-V characteristics of tested device at elevated ambient temperature were also measured and the result is shown in Figure 3.2 (b). The device was placed on a hot chuck

and the ambient temperature was changed from 30 ^{o}C to 180 ^{o}C at 25 ^{o}C interval. The saturation current density, I_{DS}, decreases rapidly with increasing T_A. For the given device, I_{DS} follows a linear relation where $I_{DS} = 0.487 - 0.0014 \times T_A$. The obtained I–V characteristics and the saturation current degradation with increasing T_A are in agreement with literature [8, 16] . The data illustrate the importance of temperature effects on performance of AlGaN/GaN HFETs.

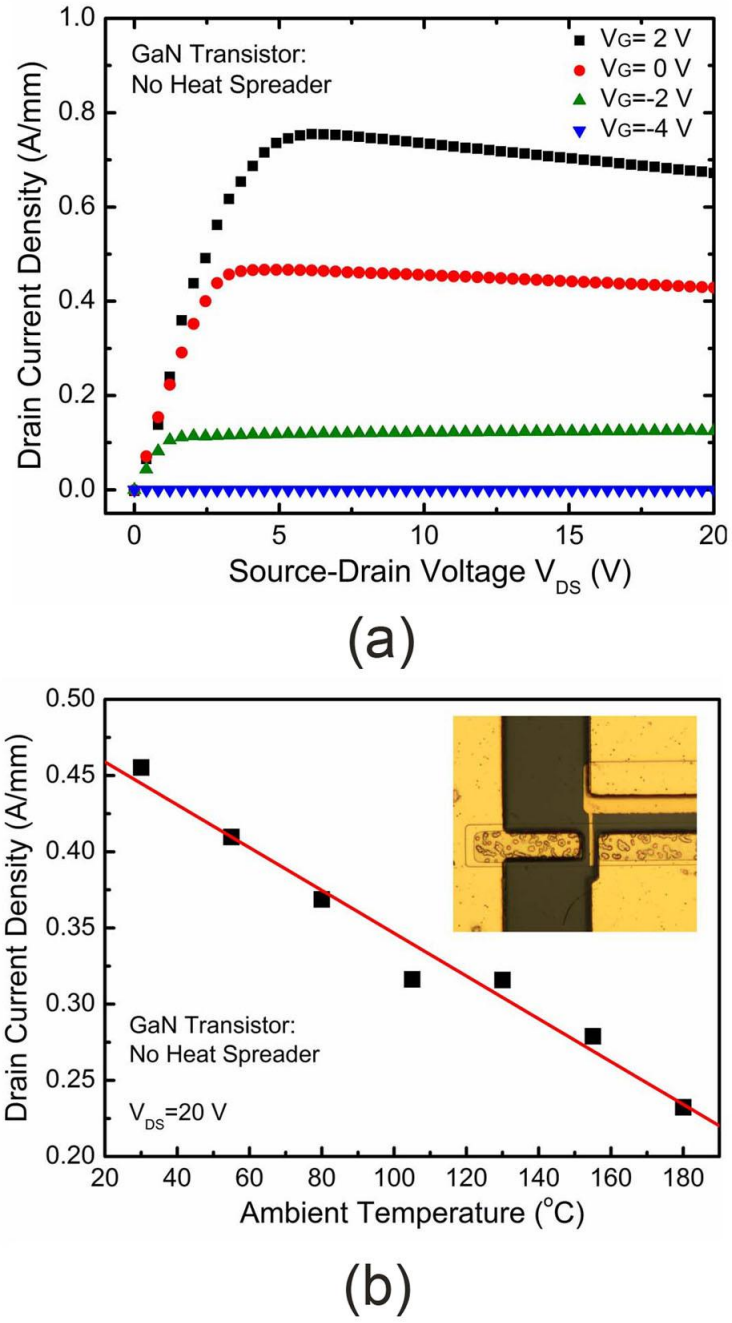

Figure 3.2 (a) DC I-V characteristics of tested AlGaN/GaN HFET device measured at room temperature. Gate bias varied from 2 V to −4 V at −2 V interval (b) Saturation current in AlGaN/GaN HFET without heat spreader biased at V_{DS} = 20 V as a function of the ambient temperature. Black squares were experimental data; Red line was obtained by linear fitting. The inset shows an optical microscopy image of AlGaN/GaN HFET.

3.3 PMMA Assisted Graphene Transfer Method

According to experimental studies and simulation results, hotspots of AlGaN/GaN HFETs are located in the source-drain opening close to the gate electrode [7]. For the thermal management applications, graphene lateral heat spreaders need to be placed accurately in predetermined locations on top of GaN devices close to the hotspots. We applied the polymethyl methacrylate (PMMA) assisted method, with some modifications. This method was first invented by Dr. Kim's group to transfer mechanically exfoliated graphene flakes onto boron nitride substrate [17]. This method is namely as PMMA assisted transfer method because PMMA membrane was utilized as supporting material for graphene films during the transfer process. Figure 3.3 shows the procedures of transferring graphene heat spreaders on AlGaN/GaN HFET device with PMMA assisted method.

First, we spin coated a layer of photoresist (Shipley 1813) with 3,500 rounds per minute (r.p.m.) on a silicon dice and baked it at 110 ℃ for 90 s. The sample was then exposed with ultraviolet light. A second layer of polymer PMMA was spin coated with 3,500 r.p.m. and baked at 130 ℃ for 90 s. Then standard mechanical exfoliation method was applied to produce graphene on the substrate from highly ordered pyrolytic graphite (HOPG). After the coating procedure, FLG films (even the single-layer graphene) can be optically identified under the microscope. For this graphene heat spreaders demonstration, we intentionally pick up FLG films with large size up to several hundred micrometers. Completing the procedure, we immersed the samples in photoresist developer ($AZ400/H_2O$ = 1:4) and dissolved the photoresist. The PMMA membranes were floated

in the liquid. We used a metal slides with a hole in the center to attach the PMMA membranes. Note that the locations of the FLG films were roughly estimated to make sure that they fell into the holes. After removing the membranes from the liquid, the metal slides were mounted on a micromanipulator, which was used for alignment. We were able to see the FLG films through the hole under the optical microscope and adjust the position of the substrate to place graphene on top of the desired location. The PMMA membranes were then dissolved by hot acetone, leaving FLG films attached to the substrate.

Figure 3.4 illustrates the concept of graphene-graphite top-surface heat spreaders and Figure 3.5 provides their microscopy images. We carefully avoided short-circuiting GaN devices with graphene films, making sure that the graphene heat spreaders extend from the drains directly to the graphite heat sinks on the side of the device. The micromanipulator, utilized for the alignment, was capable of 1–2 μm spatial resolution sufficient for handling transistors with a smaller source-drain separation. An alignment tool with submicron resolution allows one to adapt this method for transferring graphene heat spreader to much smaller devices with submicron source-drain separation.

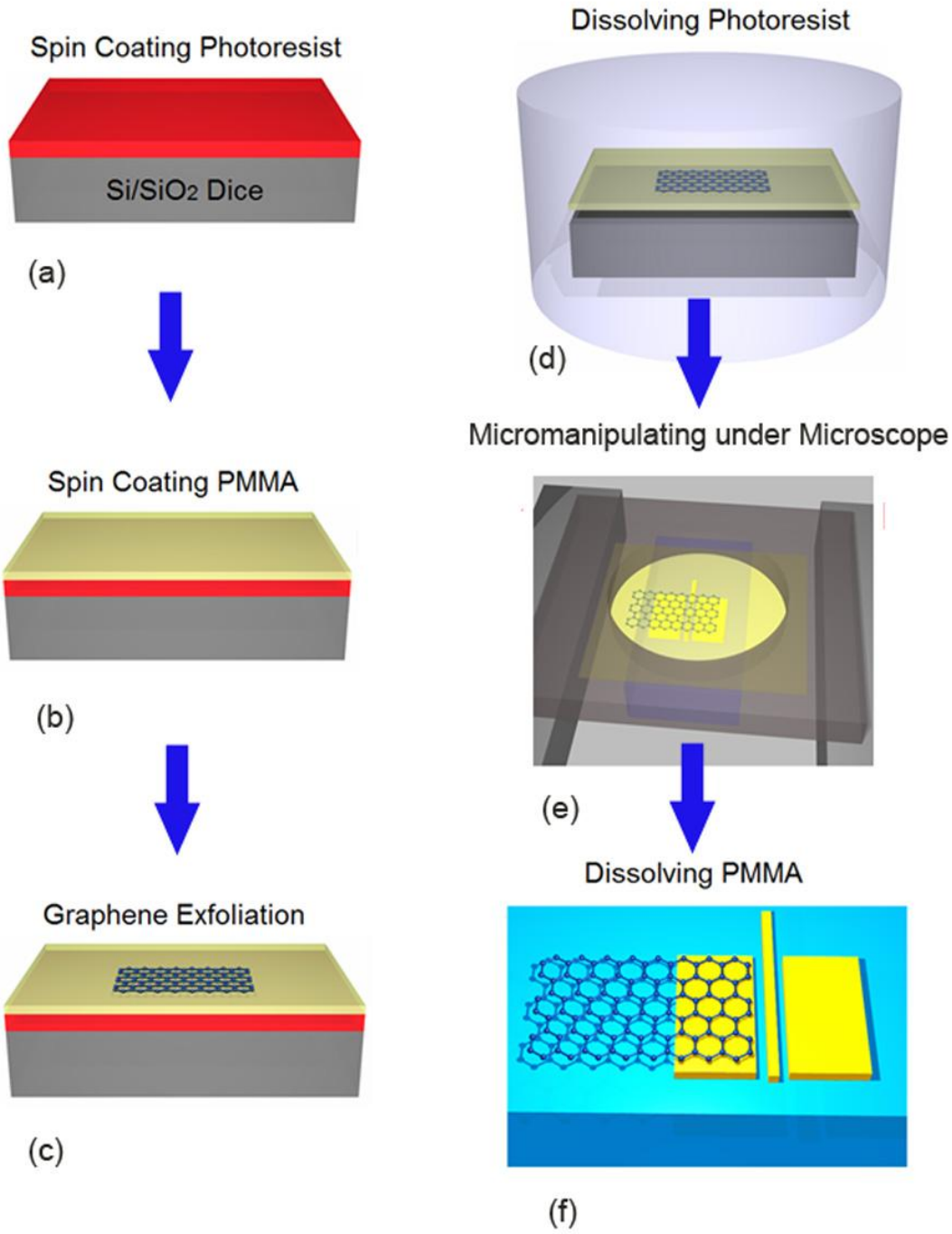

Figure 3.3 The process of transferring graphene lateral heat spreaders on top of AlGaN/GaN using PMMA assisted method. Reprinted with permission from Z. Yan, G. Liu, J. Khan and A. A. Balandin, Nature Communications, **3,** 827 (2012).

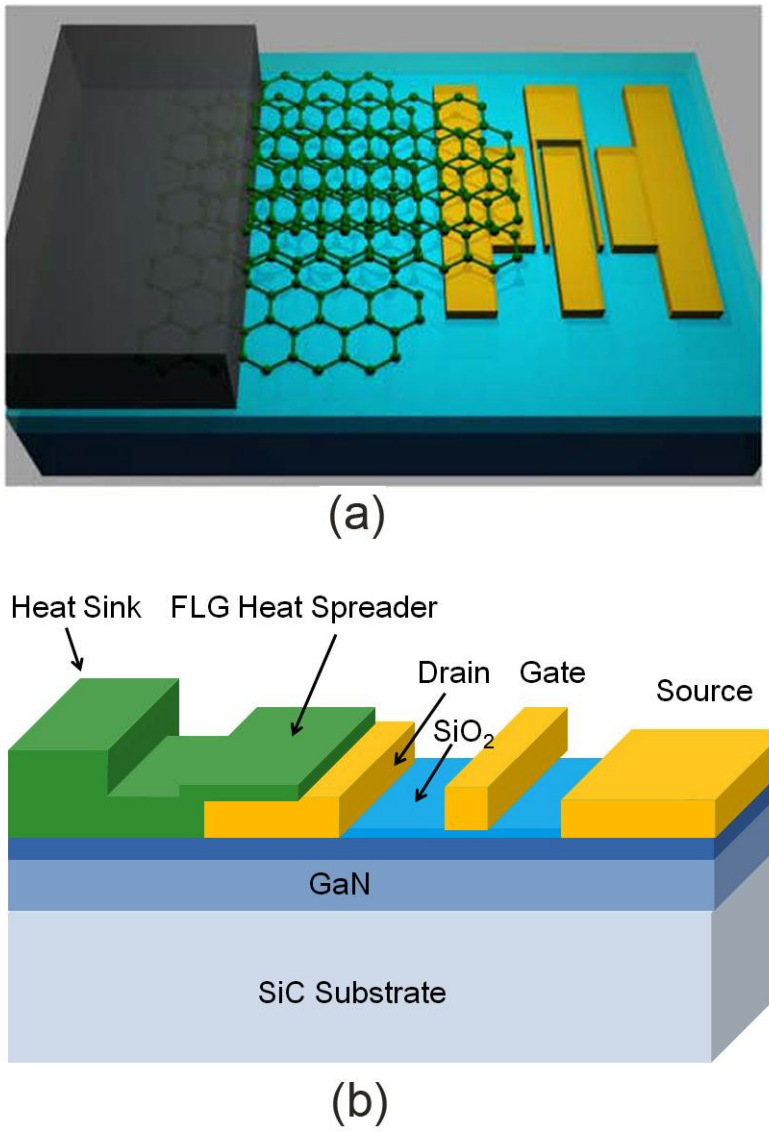

Figure 3.4 Schematics of Graphene-graphite heat spreaders for AlGaN/GaN HFETs (a) Schematic of FLG-graphite heat spreaders transferred on top of AlGaN/GaN HFET (b) Schematic of the layered device structure and the FLG-graphite heat spreaders. Dark blue color represents the AlGaN barrier layer. Reprinted with permission from Z. Yan, G. Liu, J. Khan and A. A. Balandin, Nature Communications, **3,** 827 (2012).

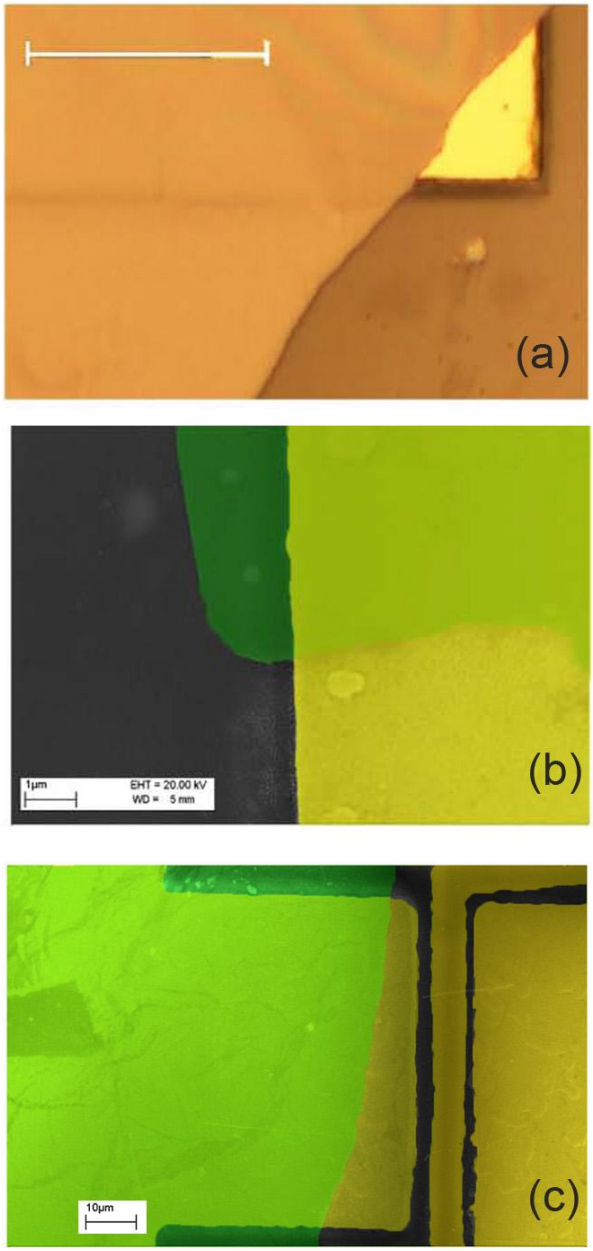

Figure 3.5 Microscopy images of FLG heat spreaders attached to AlGaN/GaN HFET (a) Optical microscopy image of the graphene films overlapping the metal contact and GaN surface demonstrating the heat spreader's close contact with the surface. Scale bar is 100µm. (b) Scanning electron microscopy (SEM) image of heat spreader—metal contact region and GaN surface. Fake colors were given to different materials for better visualization. The graphene film is indicated with the green color, while metal contacts are with the yellow color. Scale bar is 1 µm. (c) SEM image of the heat spreader transferred to the drain contact. Scale bar is 10 µm.

3.4 Raman Spectra of Graphene/GaN/SiC Layered Structure

Raman spectroscopy is a non-contact and non-destructive techniques widely used for material characterization. It has been previously applied for temperature mapping of in AlGaN/GaN HFETs by measuring the temperature-dependent shifts in the Raman peak positions [7, 18] . In my dissertation work, Raman spectroscopy was utilized both for quality control of FLG and graphite films after the transfer process and for in situ monitoring of hotspots temperature, ΔT, in the powered devices.

Raman spectra of FLG transferred on AlGaN/GaN HFETs have been measured in the backscattering configuration under the 488-nm laser excitation. Figure 3.6 shows a typical spectrum from the FLG on AlGaN/GaN/SiC layered structure. The red line shows the original Raman peak intensities obtained from experimental data; The blue line shows Raman peak intensities multiplied by 10 times in order to show the details of Raman peaks with relatively low peak intensity. Characteristic Raman peaks of FLG, GaN and SiC could be clearly identified. For example, graphene G peak is around 1580 cm^{-1} and 2D band is around 2700 cm^{-1}. No D peak could be found around 1350 cm^{-1}, indicating good crystal quality of FLG film. The peaks at ~205, 610, 777 and 965 cm^{-1} are the E_2 acoustic, A_1 longitudinal acoustic, E_2 planar optical and A_1 longitudinal optical phonon modes of SiC [19]. The narrow peak at 567 cm^{-1} is E_2 mode of GaN.

The SiC E_2 peak at 777 cm^{-1} is sensitive to temperature and has been selected for monitoring temperature rise in SiC substrate. This Raman peak shifts to lower wavenumber range (red shift) with temperature rise and approximately follows a linear dependence. Temperature coefficient of the SiC E_2 peak is -0.0144 cm^{-1} [20]. The

measured ΔT corresponds to the top part of SiC substrate—near the GaN channel layer because the laser beam was focused on the top surface.

The temperature dependence of GaN E_2 peak position has also been well established [21], thus GaN E_2 peak can be utilized for monitoring temperature rise in the GaN channel layer. The T dependence of the Raman peak position of GaN E_2 peak can be described as:

$$\omega(T) = \omega_0 - \frac{\alpha}{\exp[\frac{\beta h c \omega_0}{k_B T}] - 1} \tag{3.1}$$

where ω_0 is the extrapolated Raman peak position at 0 K, h is Plank's constant, k_B is Boltzmann's constant, c is the speed of light, α and β are the fitting parameters.

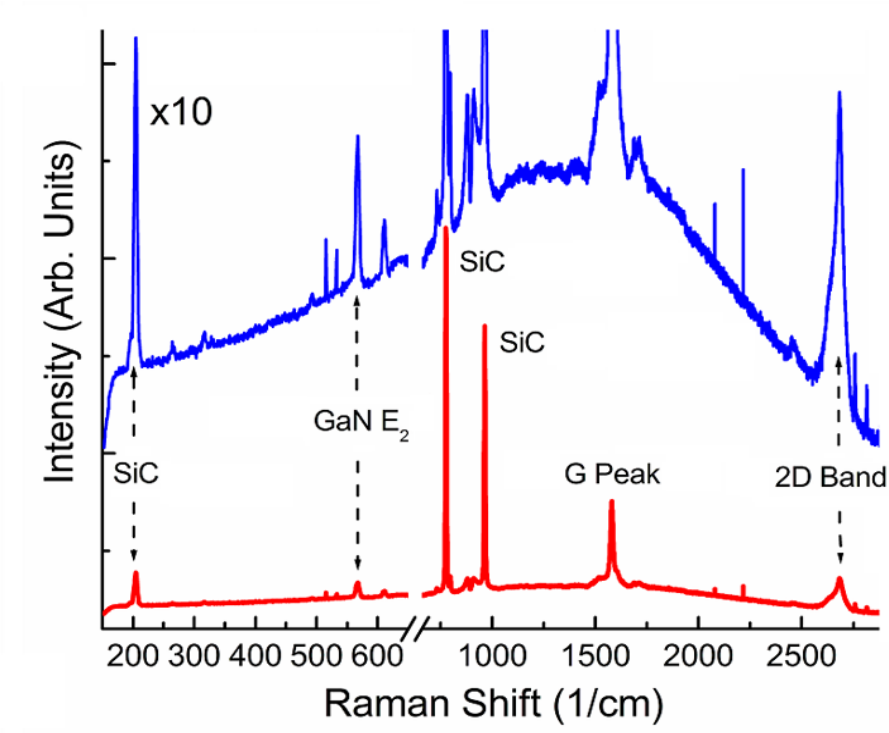

Figure 3.6 Raman spectra of FLG on top of AlGaN/GaN structure on SiC substrate.

3.5 Experimental Demonstration of Device Cooling by Graphene Heat Spreaders

The AlGaN/GaN HFETs with the heat spreaders and the reference HFETs without the heat spreaders have been wire-bonded and placed under the Raman microscope (Renishaw inVia Raman system). DC bias was applied to the tested devices and temperature rise, ΔT, due to self-heating in the device channel was monitored by the Raman peak positions. The laser spot size was ~1 μm. Laser power on the sample surface was well below ~2 mW. As GaN and SiC are wide-bandgap semiconductors, most of the laser light (wavelength 488 nm) goes through the substrate without absorption. Our measurements indicated that taking into account the light reflection, the heating due to light absorption was on the order of ~0.2 mW. Thus, the laser-induced local heating was negligible compared with the power dissipated by the transistors (above ~10 W/mm).

Figure 3.7 shows GaN E_2 phonon peak in the Raman spectra of two AlGaN/GaN devices with and without the heat spreaders. The devices were located on the same wafer and had the same layered structure and dimensions. The laser spot was focused at the channel region between the gate and the drain, closer to the gate, where ΔT is expected to be the highest. The source-drain bias, V_{DS}, was varied from 0 to ~20 V with the 4V intervals. The Raman peak position shifted to lower wavenumbers with increasing V_{DS}, indicating temperature rise with increasing dissipation power due to Joule heating effect. At the power density, P, of ~12.8 W/mm, the temperature rise, ΔT, was 92 ℃ for the AlGaN/GaN HFET with the graphene–graphite heat spreaders and ΔT = 118 ℃ in the HFET without the heat spreader. In this specific example, the same P was achieved in the

latter devices at 22 V due to small variations in the current–voltage characteristics (I–V). The corresponding ΔT measured in the top region of SiC substrate was 44 and 30 ℃ in the HFETs without and with the heat spreader, respectively. Our experimental data indicate that even at the moderate P, the graphene–graphite heat spreaders can help to reduce the hotspot temperature in AlGaN/GaN HFETs

The effective improvement of the heat removal capability of AlGaN/GaN HFETs by graphene-graphite heat spreaders and resulting device temperature reduce directly improve the I-V performance of tested device at high power density. Figure 3.8 provides direct comparison of I–V characteristics of the HFETs with (solid lines) and without (dashed lines) graphene–graphite heat spreaders. At V_G = 2 V, I_{DS} increased from 0.75 A/mm to 0.84 A/mm, 12% improvement as a result of better heat removal with the top lateral heat spreaders. At V_G = 0 V, I_{DS} increased from 0.47 A/mm to 0.51 A/mm, which is 8% improvement. At V_G = −2 V, the current density almost remained the same after introduction of the heat spreader owing to the low dissipation power density at this negative gate bias. These experiments present a direct evidence of the improvement in the AlGaN/GaN HFET I-V performance with the top-surface heat spreaders.

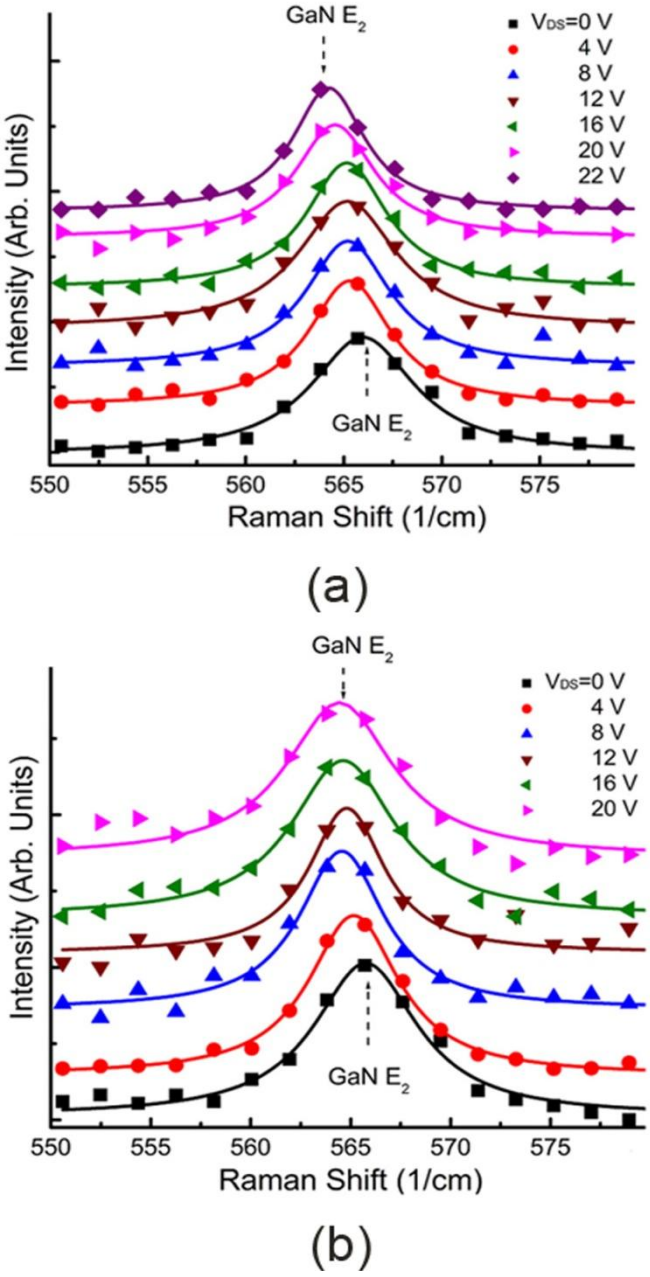

Figure 3.7 GaN E_2 peak shift in AlGaN/GaN HFET at different source-drain bias. (a) Without graphene heat spreaders (b) With graphene heat spreaders. Smaller Raman peak position shift corresponds to lower device temperature rise.

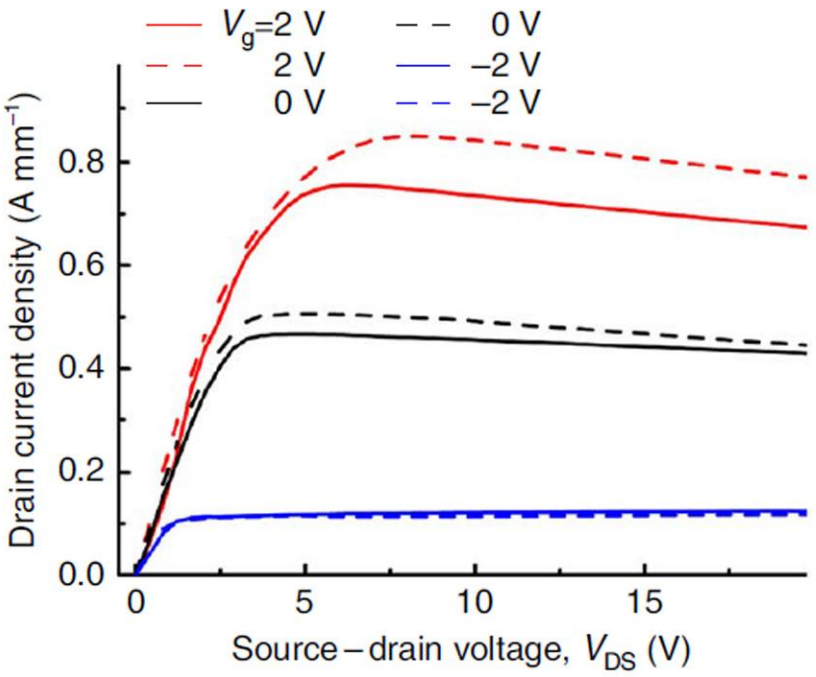

Figure 3.8 Comparison of I-Vs of AlGaN/GaN HFETs with (dashed lines) and without (solid lines) graphene heat spreaders.

3.6 Numerical Simulation of Heat Dissipation in AlGaN/GaN HFETs

I simulated the heat dissipation in the investigated AlGaN/GaN HFETs device structure with and without graphene heat spreaders and compared the simulation results with experimental data. The simulation was based on a finite element analysis method accomplished by COMSOL software. Heat conduction was modeled by numerically solving Fourier's law, $-\nabla\cdot(K\nabla T)=Q$, where Q is the heat source, defined as the heat generated within a unit volume per unit time, T is the absolute temperature, and K is the thermal conductivity. Known the geometry of simulated device structure, the amount of

heat generated, thermal conductivities of each layers and the boundary conditions, numerical simulation could generate temperature profile in the investigated device structure.

The schematic of simulated device structure is as shown in Figure 3.4. The overall dimension of the simulation domain in the direction of the device channel was 600 μm , which is much larger than the device feature size. The thickness of SiC, GaN, AlGaN and SiO_2 layers were 400 μm, 500 nm, 30 nm and 10 nm, respectively. Their corresponding thermal conductivities were taken from literature to be K = 350, 160, 120 and 1.4 W/mK, respectively. Thermal conductivity of FLG was assumed to be 2,000 W/mK . Thermal boundary resistance (TBR) at the GaN-SiC interface has an important role in self-heating effects of the AlGaN/GaN HFETs [22]. The TBR value used here was 1.5×10^{-8} m^2K/W which is consistent with reported data [23,24].

To make sure that the assumed K-values for the layers are reasonable, we measured the effective thermal conductivity of the whole AlGaN/GaN/SiC device structure. The measurements were performed using the 'laser-flash' technique. The effective K for the whole structure was measured as 300 ± 56 W/mK at RT. This value is in line with the data calculated from each individual layer with the assumed thermal conductivities and taking into account the contributions of TBR at GaN/SiC interfaces.

The thickness of the gate electrode was 120 nm and the thickness of the drain and source electrode was 240 nm. Considering that the main component of the electrodes was gold, we used K = 320 W/mK at RT. The heat source had rectangular shape with the 4-μm width and 10-nm thickness. It was placed at the interface of AlGaN and GaN layers,

at the drain-gate opening, near the gate side. TBR at GaN–substrate interface affects self-heating effect in GaN transistors. TBR was modeled with a virtual thermal isolation layer of the small thickness, *h*, between the GaN channel and SiC substrate. The effective thermal conductivity of this layer was defined as $K = h/R_B$, where R_B is TBR at the GaN–SiC interface.

The heat diffusion was simulated by numerically solving the Fourier's equation with proper boundary conditions. The bottom of SiC substrate and the left side of graphene heat spreader were kept at a constant temperature $T_0 = 25$ ℃. Other external boundaries were modeled as adiabatic condition.

I simulated heat distribution in AlGaN/GaN HFETs with and without graphene heat spreaders at P =12.8 W/mm and the results are shown in Figure 3.9. Without graphene heat spreaders, simulation gave ΔT = 119 ^{o}C for the hotspot, which is in excellent agreement with the measured ΔT = 118 ^{o}C. With graphene heat spreaders, the simulated ΔT = 102 ^{o}C is in agreement with the experimental data within ~10% uncertainty.

With this validated model we can test different graphene-graphite heat spreaders and optimize our designs. During the experimental demonstration, limited by the size of graphene-graphite heat spreader, the lateral heat sink is several hundred micrometers away from the hotspots. In principle, the same device structures with closely located heat sinks might offer higher temperature reduction. We simulated a FLG with number of atomic layer n = 10 as heat spreader and the heat sink was located at a distance, D , of 10 μm and 1 μm from the drain contact. The results are shown in Figure 3.10.

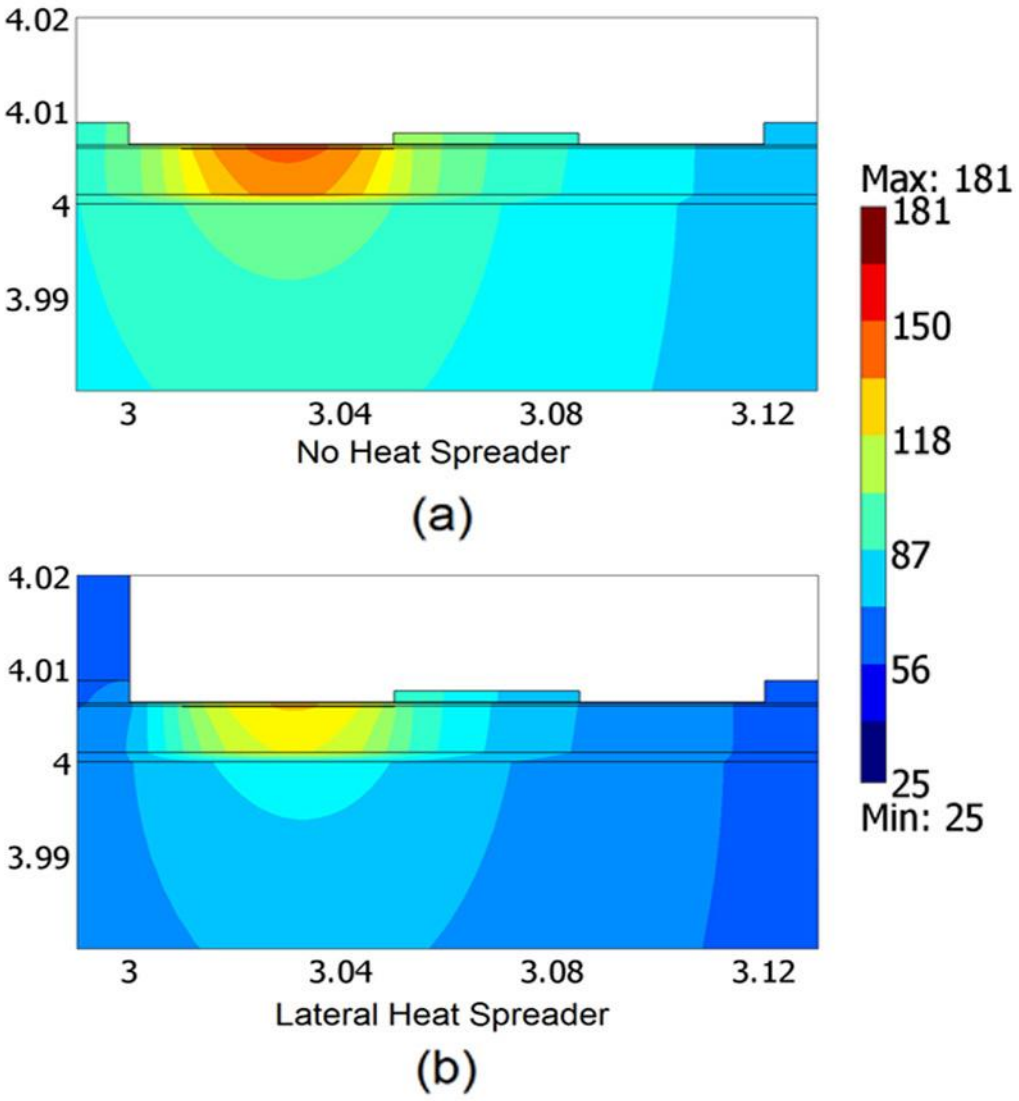

Figure 3.9 Simulated temperature profiles in AlGaN/GaN HFETs at dissipation power P = 12.8 W/mm. (a) With graphene-graphite heat spreaders. Maximum T = 144 ^{o}C, ΔT = 119 ^{o}C. (b) Without heat spreaders. Maximum T = 127 ^{o}C, ΔT = 102 ^{o}C.

The performance of graphene-graphite heat spreaders strongly depend on the distance between the lateral heat sink and device channel, where the hotspots locate. In the practical designs, the nearby heat sinks attached to the top-surface heat spreaders can be implemented with the vertical thermal vias. It is clear from the simulation results that

the bulk of heat still dissipates through the substrate to the bottom, which serves as a global heat sink. The role of the graphene-graphite heat spreader is to locally redistribute the dissipated power and lower the temperature of the hotspot near the drain.

The performance of graphene-graphite heat spreaders become more pronounced in AlGaN/GaN HFETs fabricated on sapphire substrate. Sapphire is a common substrate used for AlGaN/GaN HFETs fabrication, which is less expensive than SiC but has lower thermal conductivity, ~ 30 W/mk. Figure 3.11 shows the T profile in AlGaN/GaN HFETs on sapphire without (Fig. 3.11 a) and with (Fig. 3.11 b) graphene-graphite heat spreader operating at P = 3.3 W/mm. The data show that by introducing the graphene-graphite heat spreader with the heat sink at D = 10 μm, a drastic 68 ^{o}C reduction in the hotspot temperature can be achieved. The experimentally observed and computationally predicted reduction in ΔT can lead to more than an order-of-magnitude increase in MTTF of GaN HFETs.

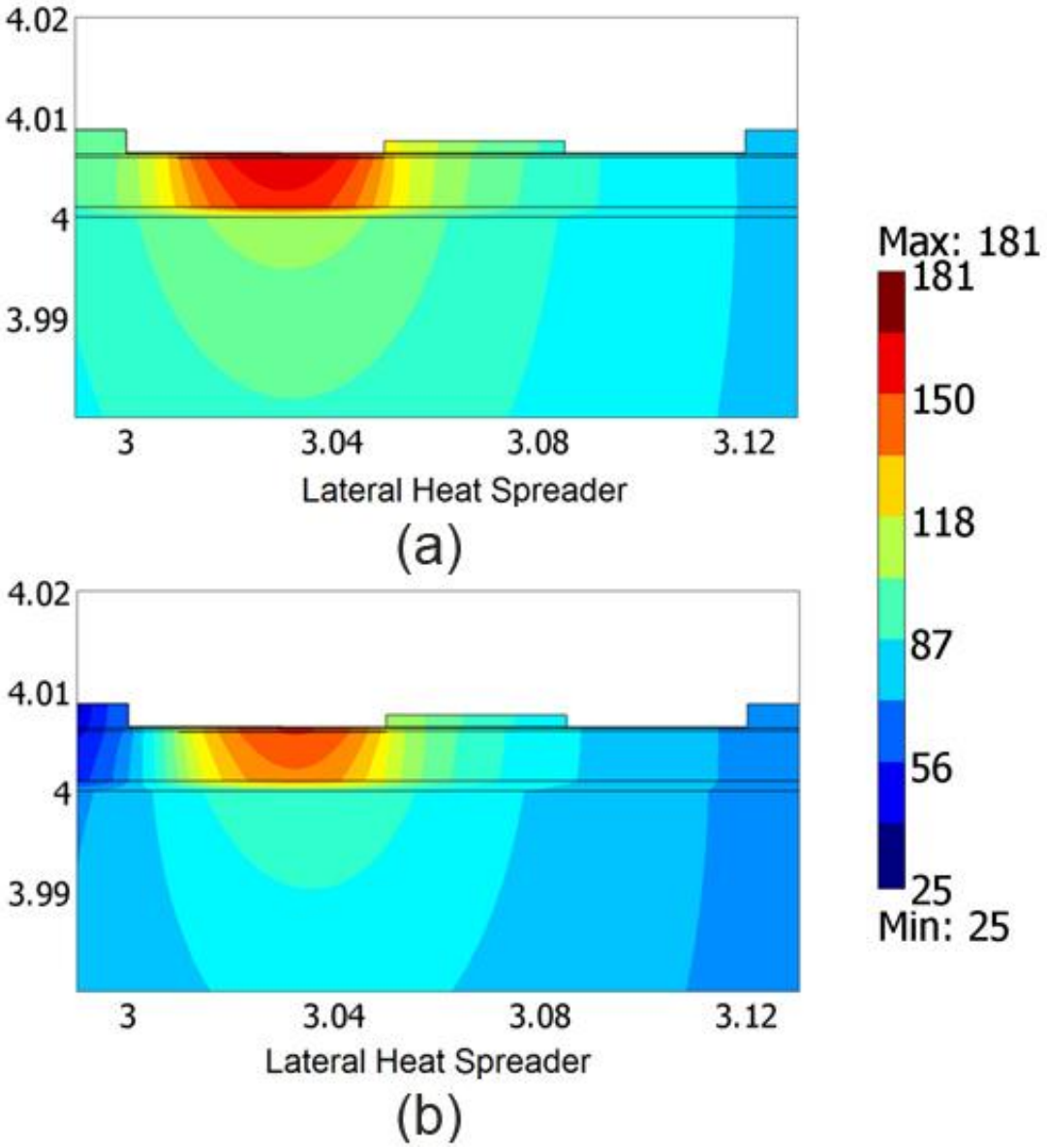

Figure 3.10 Simulated temperature profiles in AlGaN/GaN HFETs at dissipation power P = 16.8 W/mm with graphene-graphite heat spreader. (a) Heat sink located at D = 10 μm. The maximum temperature is T = 164 ℃. (b) Heat sink located at D = 1 μm. The maximum temperature is T = 150 ℃.

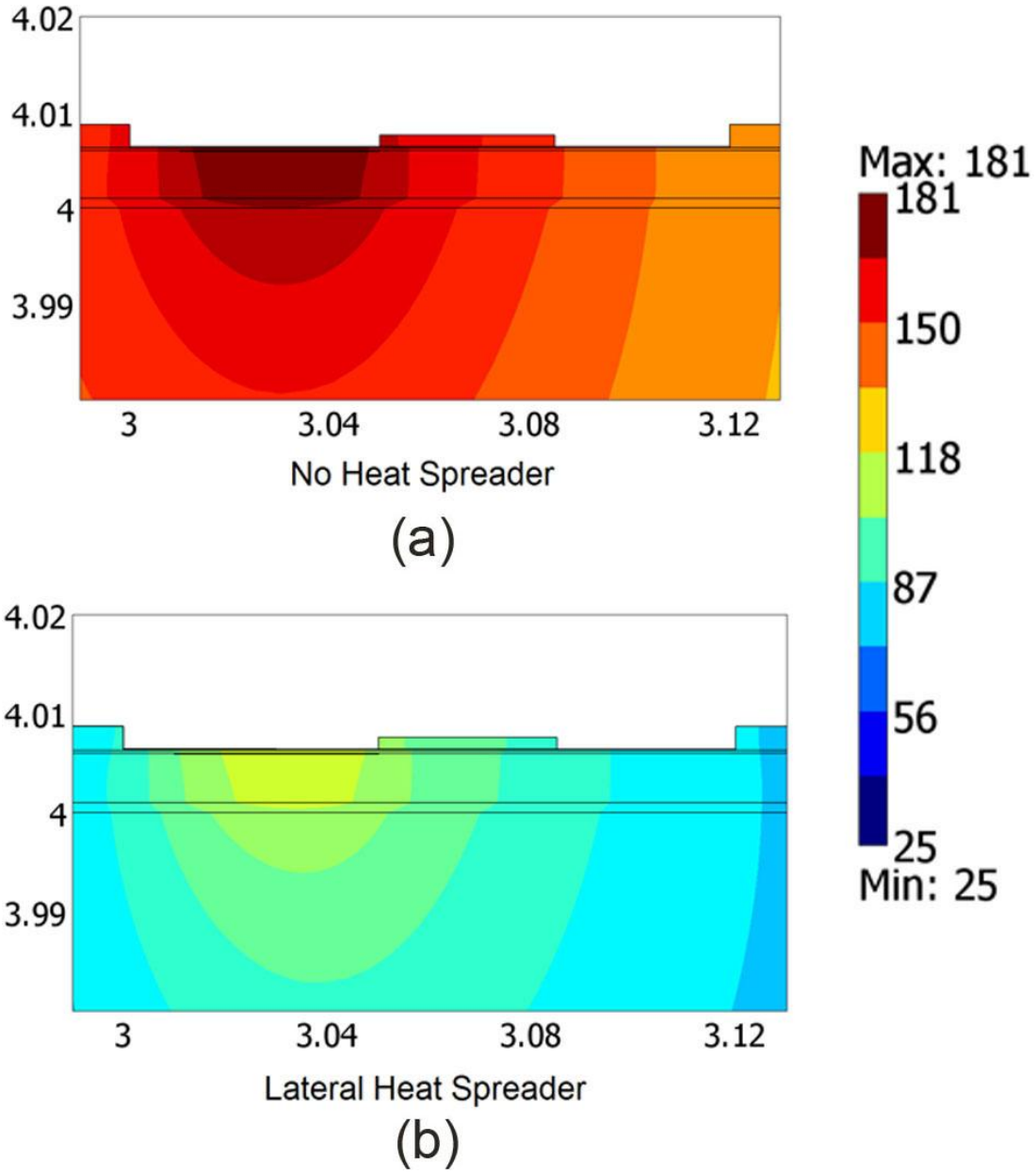

Figure 3.11 Simulated temperature profiles in AlGaN/GaN HFETs on sapphire substrate at dissipation power P = 3.3 W/mm. (a) Without graphene-graphite heat spreader. The maximum temperature is T = 181 ℃. (b) With gaphene-graphite heat spreader. The maximum temperature is T = 113 ℃.

3.7 Discussion

There are several things that I need to discuss to elucidate the scientific and technological importance of this work. With this experimental demonstration of thermal management of high-power AlGaN/GaN HFETs with graphene-graphite heat spreaders, we proposed a target-cooling idea that by placing effective lateral heat spreaders close to the hotspots of an individual device, the hotspots temperature can be reduced substantially and the device performance and reliability could be improved correspondingly. This idea is conceptually different from conventional thermal solutions which aim to reduce the overall thermal resistance of the entire device structures with packaging design. It is already well known that micrometer scale or even nonometer scale hotspots formed in the high-power electronic devices due to non-uniform heat dissipation are the reasons of thermal induced performance degradation.

We can simplify the heat dissipation in a electronic device into two steps, first heat dissipation from hotspots to nearby surroundings, then from nearby surroundings to the heat sinks. The bottle-neck of heat removal is the firsts step. Target-cooling approach implemented by lateral heat spreads aims to improve heat dissipation from hotspots to the nearby surroundings. In principle, this approach can be combined with other conventional techniques like flip-chip bonding to further improve heat removal capabilities.

For the purpose of target-cooling, heat spreaders made of high-thermal-conductivity materials with dimensions down to micrometer or even nonometer scale need to be found. Conventionally, metals have been widely used as heat spreaders and heat sinks for semiconductor devices. However, it is well known that the thermal conductivity of metal

films rapidly decreases with the film thickness [25-27]. The thermal conductivity of metal film, K_F, decreases to only ~ 20% of the bulk value, K_M, at the film thickness $H \approx 100$ nm. For example, the thermal conductivity of the gold film on etched Si for H approaching the electron mean free path $\Lambda \approx 41$ nm is $K_F \approx 0.2 \times K_B$ [27]. The expected down-scaling for aluminum films would give K_F = 26 – 48 W/mK considering that the bulk RT K_M value for aluminum ranges from ~130 to 240 W/mK, depending on its purity and quality. The drastic degradation of the heat conduction properties of metal films is due to the increased electron scattering from the rough surfaces of the films and the polycrystalline grain boundaries. The surface roughness of thin metal films is usually rather high, leading to stronger diffusive phonon scattering from interfaces.

Contrary to metals, graphene and FLG reveal high thermal conductivities at nanometer scale thin films, which is dominated by the acoustic phonons owing to the strong sp^2 bonding of their crystal lattices. It has been shown both experimentally and theoretically that the thermal conductivity of FLG is close to the bulk graphite limit of ~2,000 W/mK all the way to the few-nanometer. For this reason, the thermal conductivity of FLG is larger than that of thin metal films almost by two orders of magnitude leading to substantial differences in the heat fluxes when these materials are used as heat spreaders. The benefits of FLG as the material for heat spreaders can become even more pronounced if the isotropically pure graphene grown by the chemical vapour deposition (CVD) is used. It has been recently reported that the thermal conductivity of the isotropically engineered graphene is a factor of two higher than that of the natural graphene, which translates to an increase by ~1,000 W/mK near RT.

To compare the performance of graphene and metal heat spreaders directly, I simulated temperature profile in AlGaN/GaN HFET structure with the metal heat spreaders using our validated numerical model. Considering the best case scenario for the metal, I assumed its thermal conductivity to be 320 W/mK , which corresponds to a bulk gold or copper. The layered structure and geometry was selected to be exactly the same as in the HFETs with graphene heat spreaders. The simulation results showed that device temperature increased by ~ 10 ^{o}C in AlGaN/GaN HFET connected to metal heat spreaders compared with same device connected to FLG heat spreaders at same dissipation power. The difference in thermal management performance of FLG heat spreaders and metal heat spreaders will be even stronger if the thermal conductivity reduction in thin metal films have been taken into account.

Another thing I want to discuss is the thermal boundary resistance between graphene layer and the supporting layer underneath, the GaN layer in this case. This boundary resistance was not taken into account in the previous numerical simulation results. It was previously found that the TBR between graphene or graphite and various substrates is relatively small, on the order of 10^{-8} m^{2}K/W at RT and does not strongly depend on the interfacing material [28-30]. Our experimental results also indicate that thermal coupling between transferred FGL and the AlGaN/GaH HFET device structure is sufficient for heat transfer. It is reasonable to assume that FLG grown directly on the layered structure will have stronger thermal coupling.

The practical applications of graphene-graphite heat spreaders can be implemented with FLG grown and patterned directly on the GaN or other substrates rather than with

FLG transferred to GaN device structures. Fast progress in graphene growth by CVD and other techniques [31-33], its patterning and transferring methods, make this prospect feasible. The exotic electrical and thermal properties of graphene stimulated interest to CVD growth of FLG on various substrates, which, in turn, can make integration of FLG–graphite with various semiconductors and metals available in the near future. The proposed FLG heat spreaders can become important industry-scale thermal application of graphene and related sp^2 carbon materials. They can also provide an additional impetus for further development of the GaN-based high-frequency high-power technology.

3.8 Summary

In Chapter 3, I systematically discusses a research project of utilizing graphene-graphite heat spreaders for thermal management of high-power AlGaN/GaN HFETs. The motivation of this project lies in the sever challenge of thermal management in the designing of GaN based high-power devices. We developed a method to transfer mechanical exfoliated graphene-graphite flakes onto AlGaN/GaN HFETs with precisely controlled location to form lateral heat spreaders. Using micro-Raman spectroscopy for in situ monitoring we demonstrated that temperature of the hotspots can be lowered by ~20 ℃ in transistors operating at ~13 W/mm , which corresponds to an order-of-magnitude increase in the device lifetime. Simulations results support our experimental data and indicate that graphene-graphite heat spreaders perform even better in GaN devices on sapphire substrates. With this experimental demonstration of improved heat removal capability of high-power electronic devices via introducing lateral heat spreaders

close to the hotspots region, we proposed a target-cooling idea that aim to deal with micrometer scale or even nanometer scale hotspots directly. The proposed local heat spreading with materials that preserve their thermal properties at nanometre scale represents a transformative change in thermal management.

The major results of this project have been published in Nature Communications, Z. Yan, G. Liu, J.M. Khan and A.A. Balandin "Graphene quilts for thermal management of high-power GaN transistors"Nature Communications **3**, 827 (2012).

REFERENCES

[[1] M. A. Khan, A. Bhattarai, J. N. Kuznia, and D. T. Olson, Applied Physics Letters **63**, 1214 (1993).

[2] M. Higashiwaki, T. Mimura, and T. Matsui, Applied Physics Express **1**, 021103 (2008).

[3] J. Li, J. Cai, G. Z. Pan, Y. L. Chen, C. P. Wen, and K. L. Wang, Electron. Lett. **37**, 196 (2001).

[4] F. Yamaki, K. Inoue, N. Ui, A. Kawano, and S. Sano, in *Microwave Symposium Digest (MTT), 2011 IEEE MTT-S International*, 2011), p. 1.

[5] E. Mitani, M. Aojima, and S. Sano, in *Microwave Integrated Circuit Conference, 2007. EuMIC 2007. European*, 2007), p. 176.

[6] R. J. Trew, D. S. Green, and J. B. Shealy, Microwave Magazine, IEEE **10**, 116 (2009).

[7] A. Sarua, H. Ji, M. Kuball, M. J. Uren, T. Martin, K. P. Hilton, and R. S. Balmer, Electron Devices, IEEE Transactions on **53**, 2438 (2006).

[8] V. O. Turin and A. A. Balandin, Journal of Applied Physics **100**, 054501 (2006).

[9] S. Kidalov and F. Shakhov, Materials **2**, 2467 (2009).

[10] J. Das, H. Oprins, H. Ji, A. Sarua, W. Ruythooren, J. Derluyn, M. Kuball, M. Germain, and G. Borghs, Electron Devices, IEEE Transactions on **53**, 2696 (2006).

[11] S. Jie, H. Fatima, A. Koudymov, A. Chitnis, X. Hu, H. M. Wang, J. Zhang, G. Simin, J. Yang, and M. Asif Khan, Electron Device Letters, IEEE **24**, 375 (2003).

[12] J. Zou, D. Kotchetkov, A. A. Balandin, D. I. Florescu, and F. H. Pollak, Journal of Applied Physics **92**, 2534 (2002).

[13] W. Liu and A. A. Balandin, Journal of Applied Physics **97**, 073710 (2005).

[14] M. A. Khan, X. Hu, A. Tarakji, G. Simin, J. Yang, R. Gaska, and M. S. Shur, Applied Physics Letters **77**, 1339 (2000).

[15] G. Simin, X. Hu, N. Ilinskaya, J. Zhang, A. Tarakji, A. Kumar, J. Yang, M. A. Khan, R. Gaska, and M. S. Shur, Electron Device Letters, IEEE **22**, 53 (2001).

[16] E. R. Heller and A. Crespo, Microelectronics Reliability **48**, 45 (2008).

[17] C. R. Dean, A. F. Young, MericI, LeeC, WangL, SorgenfreiS, WatanabeK, TaniguchiT, KimP, K. L. Shepard, and HoneJ, Nat Nano **5**, 722 (2010).

[18] M. Kuball, J. M. Hayes, M. J. Uren, T. Martin, J. C. H. Birbeck, R. S. Balmer, and B. T. Hughes, Electron Device Letters, IEEE **23**, 7 (2002).

[19] J. C. Burton, L. Sun, F. H. Long, Z. C. Feng, and I. T. Ferguson, Physical Review B **59**, 7282 (1999).

[20] R. Han, B. Han, D. H. Wang, and C. Li, Applied Physics Letters **99**, 011912 (2011).

[21] M. S. Liu, L. A. Bursill, S. Prawer, K. W. Nugent, Y. Z. Tong, and G. Y. Zhang, Applied Physics Letters **74**, 3125 (1999).

[22] V. O. Turin and A. A. Balandin, Electronics Letters **40**, 81 (2004).

[23] J. Kuzmik, S. Bychikhin, E. Pichonat, C. Gaquière, E. Morvan, E. Kohn, J.-P. Teyssier, and D. Pogany, International Journal of Microwave and Wireless Technologies **1**, 153 (2009).

[24] A. Sarua, H. Ji, K. P. Hilton, D. J. Wallis, M. J. Uren, T. Martin, and M. Kuball, Electron Devices, IEEE Transactions on **54**, 3152 (2007).

[25] P. Nath and K. L. Chopra, Thin Solid Films **20**, 53 (1974).

[26] G. Chen and P. Hui, Applied Physics Letters **74**, 2942 (1999).

[27] G. Langer, J. Hartmann, and M. Reichling, Review of Scientific Instruments **68**, 1510 (1997).

[28] Y. K. Koh, M.-H. Bae, D. G. Cahill, and E. Pop, Nano Letters **10**, 4363 (2010).

[29] K. F. Mak, C. H. Lui, and T. F. Heinz, Applied Physics Letters **97**, 221904 (2010).

[30] A. J. Schmidt, K. C. Collins, A. J. Minnich, and G. Chen, Journal of Applied Physics **107**, 104907 (2010).

[31] K. S. Kim, Y. Zhao, H. Jang, S. Y. Lee, J. M. Kim, K. S. Kim, J.-H. Ahn, P. Kim, J.-Y. Choi, and B. H. Hong, Nature **457**, 706 (2009).

[32] X. Li, W. Cai, J. An, S. Kim, J. Nah, D. Yang, R. Piner, A. Velamakanni, I. Jung, E. Tutuc, S. K. Banerjee, L. Colombo, and R. S. Ruoff, Science **324**, 1312 (2009).

[33] S. Amini, J. Garay, G. Liu, A. A. Balandin, and R. Abbaschian, Journal of Applied Physics **108**, 094321 (2010).

Chapter 4 Raman Spectroscopy and Thermal Properties of Graphene Nanoribbons Encapsulated in Single-Walled Carbon Nanotubes

A novel nanotructured material- graphene nanoribbons (GNRs) encapsulated in single-walled carbon nanotubes (SWCNTs) has been synthesized using thermal induced fusion of coronene and perylene molecules. Raman spectrum of GNRs-inside-SWCNTs have been studied and the temperature coefficients of G band and 2D band have been measured. Using a modified Raman optothermal technique, thermal conductivities of thin films consisting of GNRs-inside-SWCNTs have been measured in the range of 30~50 W/mk. Theoretical considerations suggest that this novel structured material could be promising fillers for thermal interface material.

4.1 Novel Nanotructured Material- GNR Encapsulated in SWCNTs

Recently, a novel nanostructured material - graphene nanoribbons (GNR) encapsulated inside individual single-walled carbon nanotubes (SWCNTs) has been synthesized [1]. First principal simulations suggest that the electronic structure of the GNRs-inside-SWCNTs remains the same as in the free-standing GNRs indicating possible applications in nanoelectronics and photonics. The material can be prepared in the form of a thin film deposited on various substrates. The thermal properties of GNR encased inside SWCNTs can vary greatly depending on various structural parameters. In this chapter, I report the

experimental studies of Raman spectroscopy and thermal conductivities of the thin films consisting of the entangled SWCNTs with GNRs encased inside them. The films were placed on thermally insulating fused silica substrates. The measurements were performed using a modified Raman optothermal technique [2]. The Raman spectrum of GNRs-inside-SWCNTs thin films revealed the G peak and 2D band typical for sp^2-bonded carbon allotropes together with the radial breathing mode (RBM), which is a unique feature of SWCNT. The temperature coefficients of the Raman G peak and 2D band were determined by measuring Raman spectrum at the low-power excitation levels and varying the temperature of the samples externally in a cold-hot cell. Then the excitation power of the Raman laser was increased to induce local heating. The local temperature rise due to laser heating was calculated from the shift in the Raman peak positions. Finite element analysis method with COMSOL software was performed to simulate heat diffusion in the studied sample structure and the thermal conductivity value were extracted by data fitting . It was found that the thermal conductivity of the GNR-inside-SWCNTs thin film is in the range of ~ 30 – 50 W/mK. This value is similar to the thermal conductivities measured in thin films made of conventional randomly entangled CNTs. Theoretical considerations suggest that GNRs encased inside SWCNTs can be promising fillers for the thermal interface materials [3].

The sample of graphene nanoribbons encapsulated in SWCNTs were synthesized using thermal induced fusion of coronene and perylene molecules. Coronene is a large polycyclic aromatic hydrocarbon (PAH) molecule which consists of six carbon hexagons fused into a ring whereas perylene consists of five hexagon rings. SWCNTs provided

one-dimensional geometry restriction that the molecules had to be aligned in this direction to form graphene nanoribbons. SWCNTs were synthesized by aerosol CVD method based on CO decomposition on iron particles produced by pyrolysis of ferrocene vapour as described elsewhere [4]. SWCNTs were transferred as thin film onto fused silica substrate and opened using 3 steps oxidation treatment: (1) 30 min annealing on air at 380 oC; (2) removal of Fe catalyst using 15 min treatment with 15% solution of HCl (3) second annealing at 380 ^{o}C for 30 minutes. Opened SWCNTs were loaded with coronene powder (Sigma Aldrich, 97%) in stainless steel containers sealed under argon in glove box (0.5 ppm air and 1.5 ppm water) at ambient pressure. The containers were subjected to heat treatment at 450 ^{o}C for 24 hours. Residual unreacted coronene was removed by 24 hours washing in toluene and then the sample was additionally annealed under 60 Bar hydrogen gas at 750 ^{o}C in order to sublimate away dicoronylene and to remove other carbon contaminations form outer surface of nanotubes. Those samples were synthesized at the Department of Physics, Umeå University, Sweden and provided to us for Raman spectroscopy and thermal studies. More details about the synthesis of this sample could be found in reference [1].

Figure 4.1 (a) shows the schematics of a individual SWCNTs with GNR encased . The structures of coronene and perylene molecules are shown in Figure 4.1 (b) together with the suggested structures of nanoribbons formed using coronene and perylene precursors. Since these thermal induced fusion reactions took place in quasi-one-dimensional SWCNT, those coronene and perylene molecules were forced to align along the direction of CNT tube and form graphene nanoribbons.

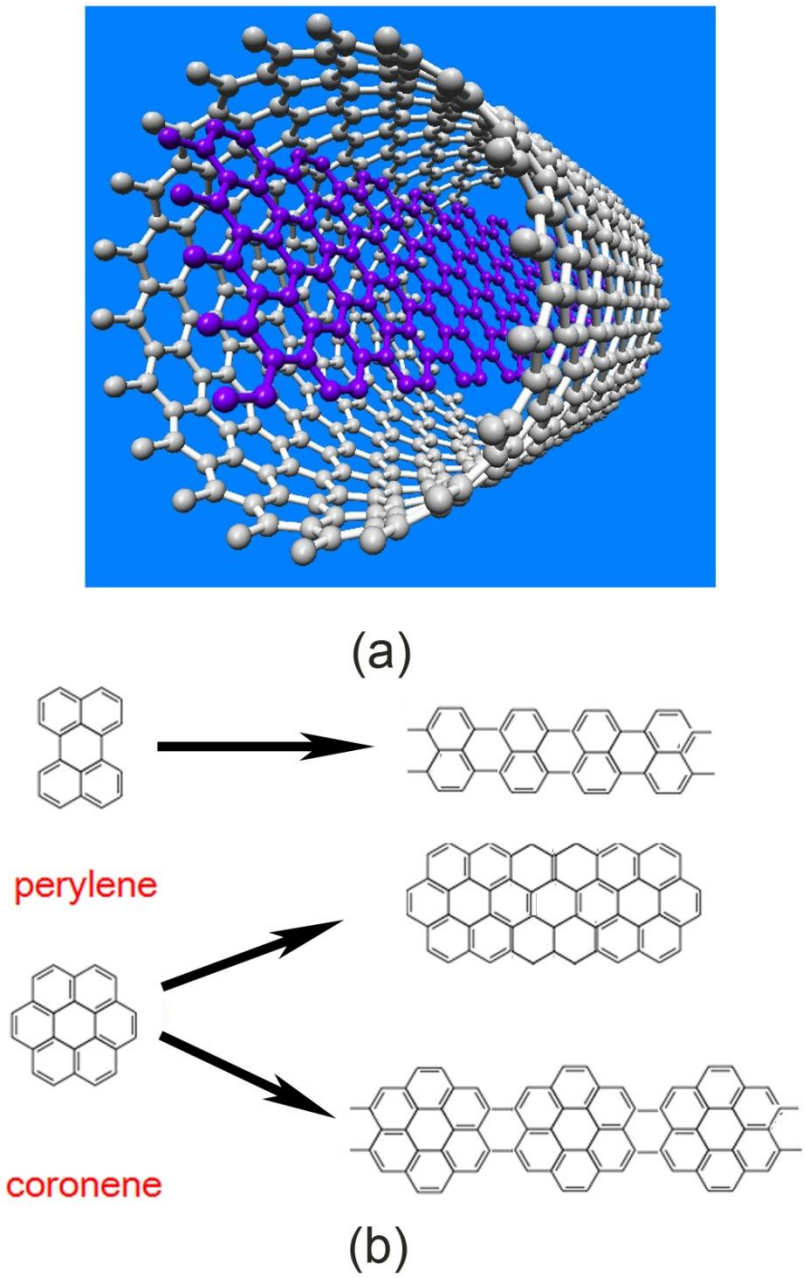

Figure 4.1 (a) Schematics of individual SWCNT with graphene nanoribbon encased. Both SWCNT and GNR consist of sp^2 bonded carbon atoms. Here white color and purple color are introduced to distinguish the carbon atoms in SWCNT and GNR (b) Structures of perylene and coronene molecules and suggested nanoribbons forming with them.

The optical microscope image of the studied thin film on silica substrate has been shown in Figure 4.2. Scale bar is 100 μm. Large area, on the order of few hundred μm^2, thin film of uniform surface could be seen. The thickness of this thin film was measured by a profilometer to be around 110 nm.

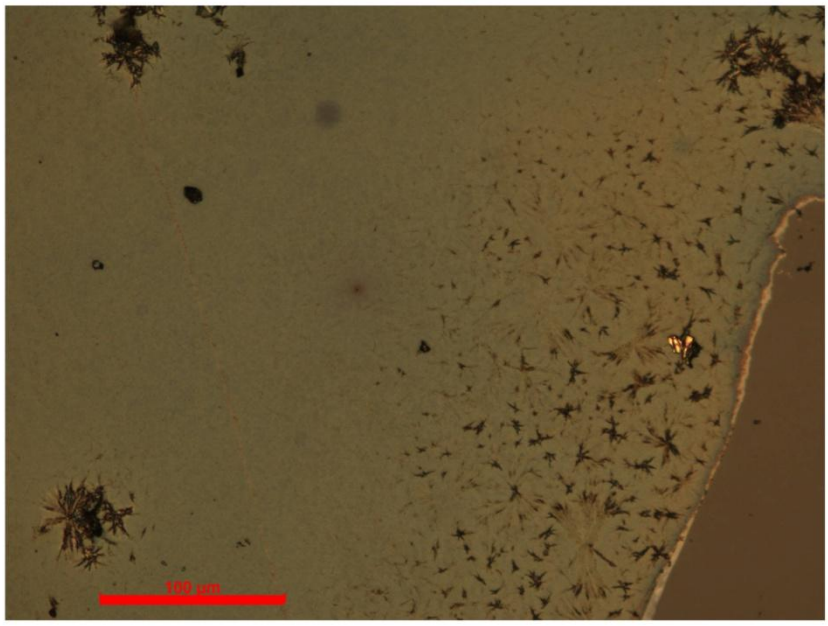

Figure 4.2 An optical microscope image of the thin film of GNRs-inside-SWCNTs on silica substrate. Scale bar is 100 μm.

4.2 Raman Spectroscopy of GNRs Encapsulated in SWCNTs

Raman spectroscopy is a powerful tool in the study of sp^2 bonded carbon allotropes including carbon nanotubes and graphene [5-7]. It has been demonstrated that micro-Raman spectroscopy can be used for unambiguous and high-throughput identification of the exact number of the graphene layers [7] which is essential for graphene based device

fabrication and applications. Micro-Raman spectroscopy could also be applied to monitor local temperature rise and measure thermal conductivity of graphene [8-10] and carbon nanotubes [11].

Raman spectra of graphene nanoribbons encapsulated in SWCNTs were studied and the measurement was carried out using a Renishaw micro-Raman spectrometer in the backscattering configuration under 488 nm laser excitation. Figure 4.3 (a) shows the obtained Raman spectrum of SWCNTs with graphene nanoribbons encased. This spectrum is very typical for sp^2 bonded carbon allotropes and it's dominated by the Raman signals of SWCNTs. The d band around 1350 cm^{-1}, G band around 1580 cm^{-1} and 2D band around 2640 cm^{-1} could be found in the spectrum as well as radial breathing mode (RBM) around 200 cm^{-1}, which corresponds to the radial expansion-contraction of nanotube. And from the peak position of RBM we can estimate that diameter of SWCNTs contained in this film is around 1.3 nm [5]. Figure 4-3 (b) shows the zoomed in spectrum around G band. G band splits into 3 peaks, G^+ peak around 1594.6 cm^{-1}, G^- peak around 1572.2 cm^{-1} and a tiny BWF mode around 1530 cm^{-1}. The mechanism of G band splitting in the Raman spectrum of SWCNTs has been well studied before [5].

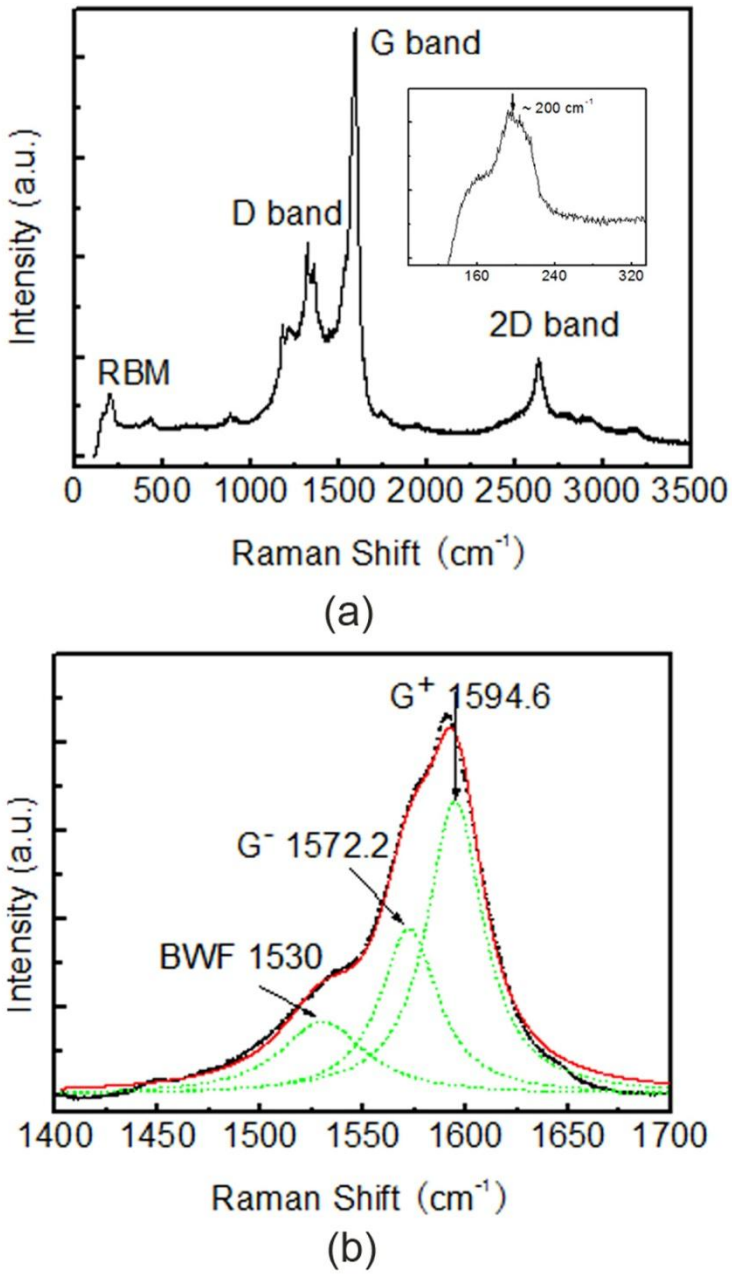

Figure 4.3 Raman spectroscopy of GNRs encapsulated in SWCNTs. (a) Raman spectrum of GNRs encapsulated in SWCNTs covering from 100 cm^{-1} to 3500cm^{-1}. Inset shows zoomed in spectrum of RBM (b) Zoomed in G band spectrum from 1400 cm^{-1} to 1700 cm^{-1}. It consists of three Lorentzian peaks. G^+ peak around 1594.6 cm^{-1}, G^- peak around 1572.2 cm^{-1} and BWF mode around 1530 cm^{-1}

The temperature dependence of the Raman peak positions of G^+ peak and 2D peak were measured in the temperature range from -80 ^oC to 110 ^oC at 10 ^oC interval and the results are shown in Figure 4.4 (a) and (b) respectively. The sample temperature was controlled externally by a cold-hot cell with 0.1 ^oC accuracy. Low laser excitation power, below 0.24 mW, was used to avoid local heating induced by Raman laser. Both G^+ peak and 2D peak positions move to lower wavenumber range, namely red shift, when the temperature keep increasing. In the measured temperature range, the temperature dependence of G^+ peak and 2D peak positions can be approximately represented by a linear relation:

$$\omega = \omega_0 + \chi T \tag{4-1}$$

where ω_0 is the frequency of Raman peak when temperature T is extrapolated to 0 K and χ is the first order temperature coefficient. The extracted temperature coefficients of G^+ peak and 2D peak are $\chi_{G^+} = -0.02$ $cm^{-1}/^oC$ and $\chi_{2D} = -0.027$ $cm^{-1}/^oC$ respectively. We can compare these results with the temperature coefficient of graphene Raman peaks and SWCNT Raman peaks which have been well studied in previous works. The temperature coefficient of G peak and 2D peak of single layer graphene are -0.016 $cm^{-1}/^oC$ and -0.032 $cm^{-1}/^oC$ [8] and the temperature coefficient of G peak of SWCNT has been measured as -0.019 $cm^{-1}/^oC$ [12]. After obtaining the temperature coefficients of G^+ peak and 2D peak, Raman spectroscopy can be used as a thermometer to measure the local temperature rise in the thin film of GNRs encapsulated in SWCNTs.

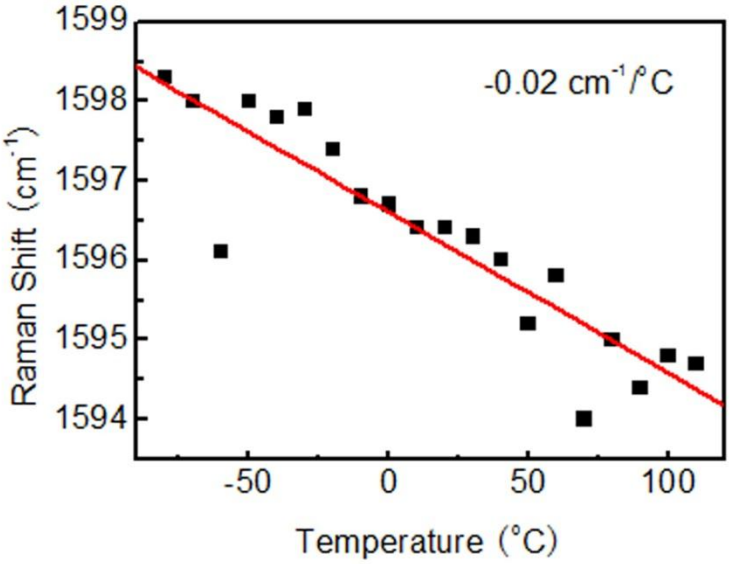

Figure 4.4 (a) Temperature dependent Raman peak shift of G^+ peak and calculated temperature coefficient. (b) Temperature dependent Raman peak shift of 2D peak and calculated temperature coefficient.

4.3 Local Heating Effects Introduced by Raman Excitation Laser

During the Raman temperature coefficients measurement, the Raman excitation power was low in order to avoid local heating introduced by laser power dissipation. In the following measurement, Raman laser excitation power was increased to 2.4 mW and the local temperature rise in the sample introduced by Raman laser was monitored by the shift of Raman peak positions. Figure 4.5 (a) and 4.5(b) compare the G band and 2D band shift at low excitation power with the Raman peak shift at high excitation power and the local temperature rise could be extracted from the difference in Raman peak positions. Raman peak position of G^+ peak shifted from 1598.7 cm^{-1} to 1594.7 cm^{-1}, from which a -4.0 cm^{-1} peak shift could be calculated . And the G^+ peak temperature coefficient, $\chi_{G^+} = -0.02$ $cm^{-1}/^oC$, was already obtained in the previous steps. Local temperature rise was extracted as 200 ^oC according to G^+ peak shift. Similarly, 2D peak shifted from 2639.6 cm^{-1} to 2634.1 cm^{-1} and temperature rise was extracted as 203 ^oC. The temperature rise calculated from 2D peak shift was consistent with the value calculated from G^+ peak shift, which could also validate the accuracy of Raman temperature coefficients measured in this work.

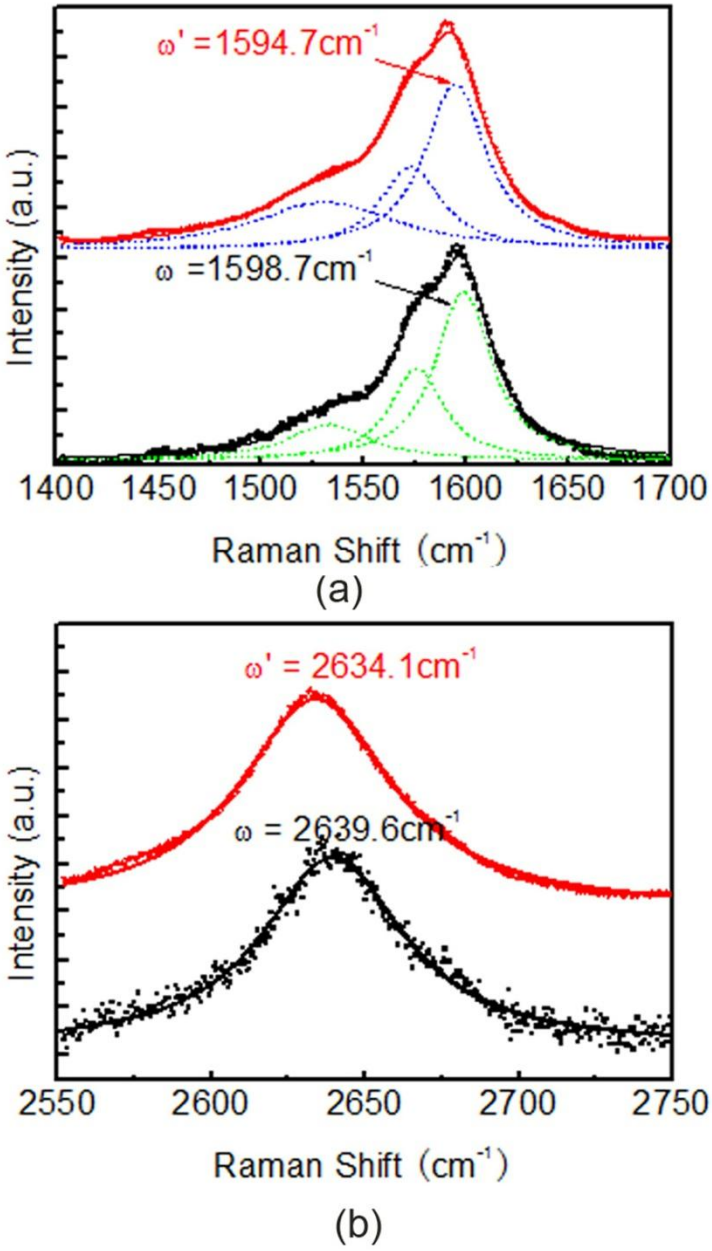

Figure 4.5 (a) G band and (b) 2D band shift induced by high intensity Raman excitation laser.

4.4 Thermal Conductivity of GNRs- inside-SWCNTs thin film

Heat dissipation in the studied sample structure was simulated by the finite element analysis method using COMSOL software and the effective thermal conductivity value of the GNRs-inside-SWCNTs thin film was extracted. The heat conduction was modeled by numerically solving Fourier's law

$$-\nabla \cdot (K\nabla T) = Q \tag{4-2}$$

where Q is the heat source, defined as the heat energy generated within a unit volume per unit time, T is the absolute temperature, and K is the thermal conductivity. Usually for the heat dissipation simulation, the heat source, which can be calculated from dissipation power, and thermal conductivity values of different material contained in the sample structure are given parameters, combined with valid boundary conditions, the temperature profile in the simulated sample structure could be obtained as the output of simulation. In this work, we tried to solve a reversed problem where temperature rise was experimentally obtained from Raman peak shift, while the thermal conductivity value of the thin film was unknown. For the given dissipation power, an initial value of thermal conductivity of the thin film was assumed to be K_0 . Numerical simulation gave a modeled temperature rise ΔT_0 and it was compared with experimental data ΔT. If ΔT_0 was larger (smaller) than ΔT, the value of thermal conductivity K was increased (decreased) in the next run until the simulated temperature rise matched the experimental data and the final value of K was obtained. The final results of numerical simulation of heat dissipation in the studied sample are shown in Figure 4.6.

The schematics of simulated device structure is shown in Figure 4.6 (a). The diameter of simulated domain is 100 μm; the thickness of GNR-inside-SWCNT film is 110 nm and the thickness of silica substrate is 1 mm. The silica substrate was placed on an ideal heat sink with temperature fixed at 300 K. Adiabatic conditions were assumed at other external boundaries. Figure 4.6 (b) shows the temperature profile on the top surface of studied sample structure and Figure 4.6 (c) shows the temperature profile on the *Zr*-cross-section of studied sample structure. The effective thermal conductivity of GNR-inside-SWCNT thin film was obtained as 41 W/mk. Similar measurements on similar samples with different film thickness gave thermal conductivity values in the range of 30~50 W/mk.

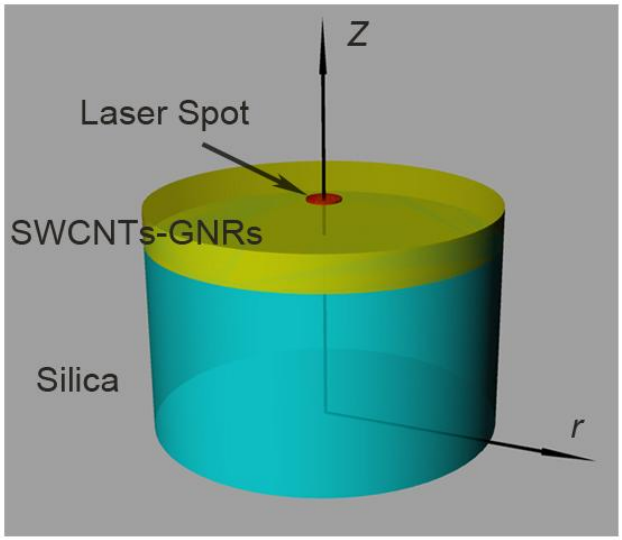

(a)

Figure 4.6 (a) Schematics of the simulated device structure. The diameter of simulated domain is 100 μm. The thickness of the silica substrate and the thin film of GNRs-inside-SWCNTs are 1 mm and 110 nm respectively.

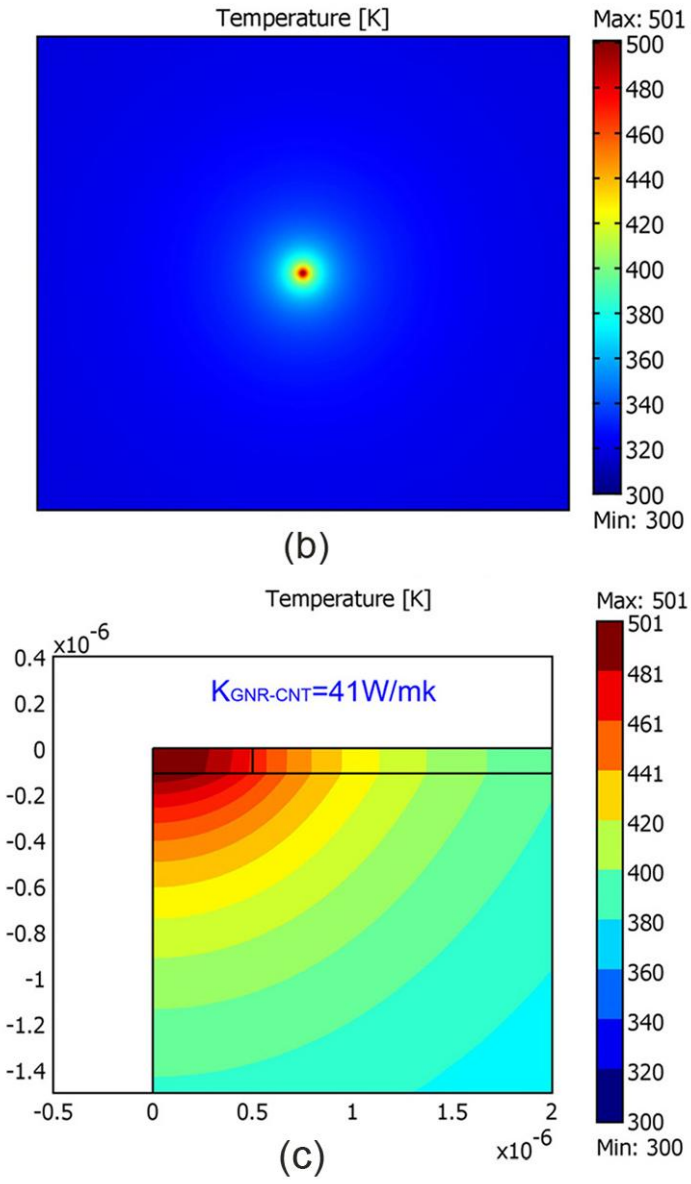

Figure 4.6 (b) Numerical simulation results of temperature profile on the top surface of the studied sample structure. The diameter of laser spot is 1 μm. (c) Temperature profile on the *Zr*-cross-section of the studied sample structure.

4.5 Discussions

Several things need to be discussed about the thermal conductivity values obtained here. Theoretical and experimental studies have revealed that thermal conductivities of sp2 bonded carbon allotropes may vary dramatically. Table 4.1 compares thermal conductivity value of GNRs-inside-SWCNTs thin film obtained in this work with the values of other sp2 bonded carbon allotropes. Individual SWCNT has high thermal conductivity at room temperature, up to 3000 W/mK. The intrinsic thermal conductivity of single-layer graphene is up to 5000 W/mK at room temperature. Thermal conductivities of graphene nanoribbons reduce to ~ 1100 W/mK due to phonon boundary scattering. From above results, it's reasonable to assume that thermal conductivity of individual SWCNT with GNRs encased will be above few hundreds. However, experimental measurement was not available with these samples. What we obtained here was the effective thermal conductivities of thin films of randomly entangled SWCNTs with GNRs encased. So the values are close to the thermal conductivities measured in two-dimensional films made of randomly entangled CNTs.

In the next step, our cooperators are trying to use some alignment method to prepare the SWCNTs, which in principle will enable the synthesis of well aligned GNRs-inside-SWCNTs samples. There are several methods reported regarding to the alignment of SWCNTs [13-15]. So hopefully the technique obstacles that we are facing in synthesizing well aligned GNRs-inside-SWCNTs will be overcome soon. Then we will use the technique established in this dissertation research to study the thermal conductivity value.

We will also attempt to measure the thermal conductivity of individual SWCNT with GNRs encased.

These novel nanostructured material may find potential applications in thermal management. Recently, graphene flakes have been proven as promising fillers for thermal interface material (TIM) [3]. Theoretical considerations suggest that GNRs encased inside SWCNTs can also be promising fillers for the TIM applications. The SWCNTs shield GNRs from external environment, which may protect GNRs from contaminations and preserve good thermal properties. Further experimental and theoretical studies are required in order to clarify the fraction of heat transported via CNTs and GNRs and the main mechanisms limiting thermal conductivity in such composite materials.

Table 4.1 Thermal conductivities of sp^2 bonded carbon allotropes

Sample	*K* (W/mk)	Method	Ref
2D films of GNRs-inside-SWCNTs	30~50	Raman Optothermal	This work
Single layer graphene	2000~5000	Raman Optothermal	[9]
Graphene nanoribbons	~1100	Electrical self heating	[16]
Individual CNT	~6600	MD simulation	[17]
Individual CNT	~3500	Electrical self heating	[18]
2D CNT film	15	Pulsed photothermal reflectance technique	[19]
2D MWCNT sheet	50	Self-heating 3ω	[20]
3D compact	4.2~2.8	Laser flash	[21]

4.6 Summary

Chapter 4 discusses the Raman spectroscopy study and thermal properties of a novel nanostrucutred material - graphene nanoribbons (GNRs) encapsulated in single-walled

carbon nanotubes (SWCNTs). These material has been synthesized using thermal induced fusion of coronene and perylene molecules. Raman spectrum of GNRs-inside-SWCNTs have been studied and the temperature coefficients of G^+ peak and 2D peak have been measured. With the obtained Raman temperature coefficients, Raman spectroscopy can be utilized as thermometer to monitor local temperature rise in the thin films of GNRs-inside-SWCNTs. Using a modified Raman optothermal technique, effective thermal conductivities of the thin films have been measured in the range of 30~50 W/mk. Theoretical considerations suggest that this novel structured material could be promising fillers for thermal interface material.

REFERENCES

[1] A. V. Talyzin, I. V. Anoshkin, A. V. Krasheninnikov, R. M. Nieminen, A. G. Nasibulin, H. Jiang, and E. I. Kauppinen, Nano Letters **11**, 4352 (2011).

[2] A. A. Balandin, Nat Mater **10**, 569 (2011).

[3] K. M. F. Shahil and A. A. Balandin, Nano Letters **12**, 861 (2012).

[4] A. Moisala, A. G. Nasibulin, D. P. Brown, H. Jiang, L. Khriachtchev, and E. I. Kauppinen, Chemical Engineering Science **61**, 4393 (2006).

[5] M. S. Dresselhaus, G. Dresselhaus, R. Saito, and A. Jorio, Physics Reports **409**, 47 (2005).

[6] P. C. Eklund, J. M. Holden, and R. A. Jishi, Carbon **33**, 959 (1995).

[7] A. C. Ferrari, J. C. Meyer, V. Scardaci, C. Casiraghi, M. Lazzeri, F. Mauri, S. Piscanec, D. Jiang, K. S. Novoselov, S. Roth, and A. K. Geim, Physical Review Letters **97** (2006).

[8] I. Calizo, A. A. Balandin, W. Bao, F. Miao, and C. N. Lau, Nano Letters **7**, 2645 (2007).

[9] A. A. Balandin, S. Ghosh, W. Bao, I. Calizo, D. Teweldebrhan, F. Miao, and C. N. Lau, Nano Letters **8**, 902 (2008).

[10] S. Ghosh, I. Calizo, D. Teweldebrhan, E. P. Pokatilov, D. L. Nika, A. A. Balandin, W. Bao, F. Miao, and C. N. Lau, Applied Physics Letters **92**, 151911 (2008).

[11] F. Huang, K. T. Yue, P. Tan, S.-L. Zhang, S. Zujin, X. Zhou, and G. Zhennan, Journal of Applied Physics **84**, 4022 (1998).

[12] N. R. Raravikar, P. Keblinski, A. M. Rao, M. S. Dresselhaus, L. S. Schadler, and P. M. Ajayan, Physical Review B **66**, 235424 (2002).

[13] P. M. Ajayan, O. Stephan, C. Colliex, and D. Trauth, Science **265**, 1212 (1994).

[14] W. Z. Li, S. S. Xie, L. X. Qian, B. H. Chang, B. S. Zou, W. Y. Zhou, R. A. Zhao, and G. Wang, Science **274**, 1701 (1996).

[15] R. Haggenmueller, H. H. Gommans, A. G. Rinzler, J. E. Fischer, and K. I. Winey, Chemical Physics Letters **330**, 219 (2000).

[16] R. Murali, Y. Yang, K. Brenner, T. Beck, and J. D. Meindl, Applied Physics Letters **94**, 243114 (2009).

[17] S. Berber, Y.-K. Kwon, and D. Tománek, Physical Review Letters **84**, 4613 (2000).

[18] E. Pop, D. Mann, Q. Wang, K. Goodson, and H. Dai, Nano Letters **6**, 96 (2005).

[19] D. J. Yang, Q. Zhang, G. Chen, S. F. Yoon, J. Ahn, S. G. Wang, Q. Zhou, Q. Wang, and J. Q. Li, Physical Review B **66**, 165440 (2002).

[20] A. E. Aliev, M. H. Lima, E. M. Silverman, and R. H. Baughman, Nanotechnology **21**, 035709 (2010).

[21] H. L. Zhang, J. F. Li, K. F. Yao, and L. D. Chen, Journal of Applied Physics **97**, 114310 (2005).

Chapter 5 Conclusions

5.1 Summary of Dissertation

Thermal management has become a severe challenge for the development of high-power density semiconductor devices. Micrometer scale or even nonometer scale hot spots may form in the active device channel, leading to device performance degradation and reliability issues. Finding new materials with high thermal conductivity as heat spreaders is an attractive approach to improve heat removal capability of modern electronic devices. Graphene is a promising candidate material for heat spreader applications.

Graphene and few layer graphene flakes have high thermal conductivity. Unlike metals, the heat transport is mainly dominated by phonons, so graghene can maintain high thermal conductivity when the thickness reduces to few nonometers. The planar two-dimensional geometry of graphene provides good compatibility of conventional lithography and etching techniques established in semiconductor industry. And the rapid progress in the chemical vapor deposition (CVD) growth of graphene has led to fabrication of large-area graphene layers that are transferable onto various substrates. It's reasonable to predict that a reliable method to synthesize high-quality large-scale graphene film will be developed in the near future and the mass production of graphene will be available in semiconductor industry. All above reasons explain why we are interested in graphene heat spreaders.

In this dissertation, we propose a target cooling approach implemented with graphene-graphite heat spreaders to improve heat removal capabilities of high-power

density electronic devices. We have made proof-of-concept demonstration on AlGaN/GaN HFET which is a example of high-power density electronic devices. Thermal management of GaN transistors can be substantially improved via introducing graphene-graphite heat spreaders, which were transferred on top of AlGaN/GaN transistors on SiC substrates. Using micro-Raman spectroscopy for in situ monitoring we demonstrated that temperature of the hotspots can be lowered by ~20 ℃ in transistors operating at ~13 W/mm , which corresponds to an order-of-magnitude increase in the device lifetime. Simulations results support our experimental data and indicate that graphene quilts perform even better in GaN devices on sapphire substrates. The proposed local heat spreading with materials that preserve their thermal properties at nanometre scale represents a transformative change in thermal management.

This dissertation also explores the Raman spectroscopy and thermal properties of a anovel nanostrucutred material - GNRs-inside-SWCNTs. This material was synthesized using thermal induced fusion of coronene and perylene molecules. Raman spectrum of GNRs-inside-SWCNTs was studied and the temperature coefficients of G^+ peak and 2D peak were measured. With the obtained Raman temperature coefficients, Raman spectroscopy can be utilized as thermometer to monitor local temperature rise in the thin films of GNRs-inside-SWCNTs. Using a modified Raman optothermal technique, effective thermal conductivities of the thin films were measured in the range of 30~50 W/mk. Theoretical considerations suggest that this novel structured material could be promising fillers for thermal interface material.

5.2 Competitive Awards Won during Dissertation Research

- **2012 Thermal Student Competition Winner** International Microelectronics Assembly and Packaging Society (IMAPS) Workshop on Thermal Management, Las Gatos, CA, Nov. 2012
- **Young Scientist Award** 38th Conference on the Physics and Chemistry of Surfaces and Interfaces (**PCSI-38**), San Diego, CA, Jan. 2011
- **Best Symposium (Oral/Poster) Presentation Award** of Symposium Y, Materials Research Society 2011 Spring meeting, San Francisco, CA, Apr. 2011

5.3 Peer-Reviewed Journals Resulted from the Dissertation Research

[1] Z. Yan, G. Liu, J. Khan and A. A. Balandin, "Graphene Quilts for Thermal Management of High-power GaN Transistors" Nature Communications 3 827 (2012)

[2] Z. Yan, G. Liu, S. Subrina and A. A. Balandin, "Experimental Demonstration of Efficient Thermal Management of High-power GaN/AlGaN Transistors with Graphene Lateral Heat Spreaders" MRS Proc. Y3.5 (2011).

[3] Z. Yan and A. A. Balandin, "Raman Spectroscopy and Thermal Properties of Graphene Nanoribbons Encapsulated in Single-Walled Carbon Nanotubes" (In preparation).

[4] J. Lin, D. Teweldebrhan, K. Ashraf, G. Liu, X. Y. Jing, Z. Yan, R. Li, M. Ozkan, R. K. Lake, A. A. Balandin, C. S. Ozkan, "Gating of Single-layer Graphene with Single-stranded Deoxyribonucleic acids" SMALL 6 No. 10 p1150 (2010)

[5] J. Lin, D. Teweldebrhan, K. Ashraf, G. Liu, X. Jing, Z. Yan, R. Li, R.K. Lake, M. Ozkan, A.A. Balandin, C.S. Ozkan, "Gating of Single-layer Graphene Using DNA" Proceedings of International Society for Optical Engineering (SPIE), San Diego, CA, Aug. 2009, N. Kobayashi, F. Ouchen, I. Rau (Chairs), Vol. 7403, 74030C (2009)

5.4 Conference Presentations Resulted from the Dissertation Research

ORAL PRESENTATION:

[1] Z. Yan, et al. "Thermal Conductivity of Thin Films Composed of Graphene Nanoribbons Encapsulated in Single-Walled Carbon Nanotubes" Materials Research Society (MRS) 2013 Spring Meeting, San Francisco, CA, Apr. 2013

[2] Z. Yan, G. Liu and A. A. Balandin, "Graphene Heat Spreaders for High-power GaN Transistors" International Microelectronics Assembly and Packaging Society (IMAPS) Workshop on Thermal Management, Las Gatos, CA, Nov. 2012

[3] Z. Yan, G. Liu, J. Khan and A. A. Balandin, "Thermal Management of GaN High-power Devices with Graphene Quilts" Materials Research Society (MRS) 2012 Spring Meeting, San Francisco, CA, Apr. 2012

[4] Z. Yan, G. Liu, D. Teweldebrhan, V. Goyal, S. Sabrina, C. M. Nolen and A. A. Balandin, “Few-layer Graphene Top-surface Heat Spreaders for High-power Electronics” PCSI-38:38th Conference on the Physics and Chemistry of Surfaces and Interfaces, San Diego, CA, Jan. 2011

POSTER PRESENTATION:

[1] Z. Yan, G. Liu, S. Subrina & A. A. Balandin, “Experimental Demonstration of Efficient Thermal Management of High-power GaN/AlGaN Transistors with Graphene Lateral Heat Spreaders” Materials Research Society 2011 Spring, San Francisco, CA, Apr. 2011

[2] Z. Yan, G. Liu, D. Teweldebrhan, V. Goyal, S. Sabrina, C. M. Nolen and A. A. Balandin, “Few-Layer Graphene Top-surface Heat Spreaders for High-Power Electronics" PCSI-38: 38th Conference on the Physics and Chemistry of Surfaces and Interfaces, San Diego, CA, Jan. 2011 –Best Poster Award

[3] G. Liu, Q. Shao, D. Teweldebrhan, Z. Yan, J. Yu, A.A. Balandin, “Noise Reduction in Graphene Transistors: Experiment and Modeling-Based Optimization” Semiconductor Research Corporation FENA Review Meeting, UCLA, Los Angeles, CA, Jan. 2009